Politecnico di Torino

Ingegneria Energetica e Nucleare – Renewable Energy Systems
A.a. 2024/2025
Sessione di Laurea Dicembre 2024

From Model to Practice: Study of Deformations in a Pressurized Vessel Using Theoretical, Experimental, and FEA Methods

Tutor:
Andrea Mura

Candidate:
Irene Curcio
Matr. 315423

Company:

Index

List of figures

List of formulas

Introduction

The prediction of the deformations that a body subjected to any stress will undergo is an essential part of the design and production process of any object. It directly influences various aspects of the design, manufacturing, and final use of a product. Deformation of a material under load can compromise the safety of the structure. If deformations are not controlled, there is a risk of malfunction or even collapse. Accurately predicting how and where deformations will occur helps ensure structural safety or predict potential failure points.

Moreover, deformations can be a significant issue for components that must meet precise dimensional tolerances. Therefore, it is essential to monitor and account for them in the design phase. The choice of material is also influenced by how it reacts to stresses. The optimal material is selected for each component to improve overall efficiency. Knowing in the design phase how the body will respond to applied loads is crucial not only for understanding its useful life (e.g., for a body subjected to cyclic loads, we could estimate the number of life cycles) but also for determining whether deformation could cause the part to lose functionality.

The focus on deformation prediction in this thesis is especially relevant to pressure vessels, as these devices are used in critical industries such as chemical, petrochemical, pharmaceutical, and nuclear sectors. The criteria mentioned earlier will be applied to these bodies. Pressure vessels are subject to high pressures that generate stresses and deformations in their components. If not correctly predicted, this could lead to severe damage, such as vessel rupture, causing dangerous leaks or explosions. To ensure safety, it's crucial to predict how the vessel material will behave under pressure by calculating the tensile stresses that develop in the walls, which can be studied using membrane theory. If the body is subjected to cyclic loading, a fatigue analysis is necessary, although this will not be covered in this work.

The shape and size of a pressure vessel must be extremely precise to ensure that critical parts like nozzles, flanges, and welds function correctly under load. Unforeseen deformations could lead to coupling issues, leakage at connections, or structural defects. The optimal choice for a pressure vessel would be a material with good fatigue resistance (for cyclic stresses), good corrosion resistance (where needed), or the ability to undergo plastic deformation. Regarding service life, particular attention must

be given to the phenomenon of creep in high-temperature conditions and structural fatigue. Material treatment processes, such as welding or stamping, also require careful attention to minimize production errors. For example, thermal deformation caused during the welding of vessel components can result in residual stresses that compromise structural integrity. FEM (Finite Element Method) simulations can predict how these stresses develop.

In conclusion, through stress and deformation analysis, it is possible to improve the lifespan, ensure dimensional tolerances, and minimize risks. Advanced simulation tools, like FEM analysis, allow for accurate predictions of vessel behavior under pressure, contributing to a more efficient and safer design.

This thesis will focus on studying the deformations experienced by a pressure vessel during pressurization and depressurization phases, analyzing them first from a theoretical perspective, then through simulation software, and finally comparing these results with those obtained experimentally in the laboratory.

The vessel used as a case study is provided by Baglioni S.p.A. Baglioni S.p.A. is an Italian company specializing in the production of pressure vessels, particularly for compressed gases. The company was founded in 1968 by Alfredo Baglioni under the original name C.M. Contenitori Metallici Srl in San Pietro Mosezzo, Novara. In 1984, the company obtained ASME certification, enabling it to sell its products in the U.S., marking its first major step towards international expansion. In 1988, Baglioni opened its first production plant in France and received CE certification after the EU's initial directive on pressure vessels, allowing distribution across Europe. In the 1990s and 2000s, the company concentrated its design and engineering activities in Novara. In 2002, Baglioni entered the Special Pressure Equipment (SPE) market, and in 2003, it opened its first production plant in China, followed by another facility in Shanghai in 2010. Today, Baglioni operates nine production facilities across three continents (Europe, Asia, and America) and employs around 1,000 people. Looking to the future, Baglioni is focusing on green hydrogen and innovation, while maintaining a commitment to sustainability and ethical business practices. *(Baglioni Group, n.d.)*

During her internship at the aforementioned company, the candidate visited the facilities, receiving explanations of all production phases for the various types of devices available. In addition, fatigue tests performed on some of these devices were demonstrated, along with a review of reports from certified bodies.

Calculation of stresses in thin vessels

General description of pressure vessels

Pressure vessels are designed to contain fluids, gases, or liquids under specific temperature and pressure conditions. They are typically subject to variations (including cyclic) in internal pressure, which differs from the ambient pressure. The construction techniques and materials chosen depend on the operating conditions, the quantity, and the type of fluid the vessel will contain. The design must not only meet the required operational characteristics but also comply with safety regulations, as the failure of a pressure vessel can be very dangerous, potentially causing gas leaks, fires, and explosions.

Vessels can be produced in various shapes, but the most common are cylindrical, spherical, and conical. Among these, the cylindrical shape is very advantageous mechanically, as it allows for equal forces in all directions. However, this type of construction might be economically disadvantageous. The shape of the vessel is usually chosen based on the application field, but in general, they always consist of closure heads, shell, nozzles, control openings, and supports. (Fig. 1)

The closure heads and the shell are the fundamental parts of the vessel responsible for maintaining the pressure. They are welded together and can have different thicknesses or materials. The nozzles and control openings are two different types of openings: the former are necessary for inspections and maintenance, while the latter have operational purposes such as fluid passage or pressure regulation. Supports are non-pressurized parts designed to keep the vessel in the desired position.

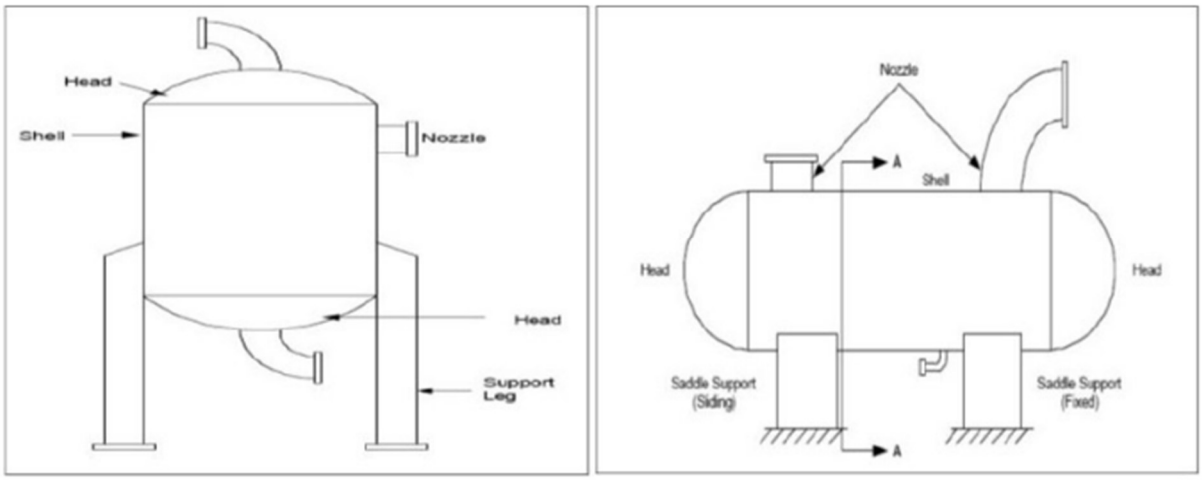

Figure 1: General diagram of a horizontal or vertical vessel.

Vessels are classified into two types based on the wall structure: solid wall vessels and multi-layered vessels. The main difference between the two is implied by their names: the multi-layered vessel has a wall characterized by several concentric layers of different diameters made of materials with different properties.

Pressure vessels are widely used across various industries for storage and processing purposes. Their applications range from gasoline storage and distillation towers to autoclaves, compressed air receivers, and nuclear reactor components.

The selection of materials for the construction of a vessel is a fundamental part of the production process and is carried out based on both the material characteristics and the operating conditions to which it will be subjected.

Pressure vessel failure can be due to various factors: the material might not comply with regulations, there could be design calculation errors, lack of safety devices such as valves, insufficient testing phase, and so on. Throughout the lifecycle of a vessel, from design to service, several causes of failure can occur:

- Material not conforming to regulations, with microstructural imperfections
- Errors in the design phase
- Insufficient testing phase
- Incorrect installation of safety devices (e.g., safety valves)
- Low quality of welds
- Errors in the production and/or assembly phase
- Incorrect use by the end customer
- Lack of maintenance
- Unauthorized modifications

The types of loads on a pressure vessel can be classified based on localization (general or local loads) (Fig. 2) or frequency of application (stationary or non-stationary) (Fig. 3).

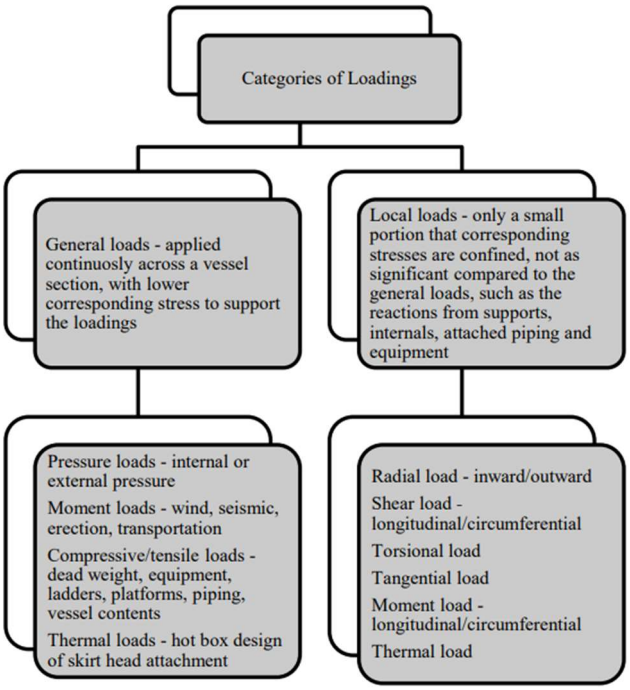

Figure 2: Categories of loadings based on localization.

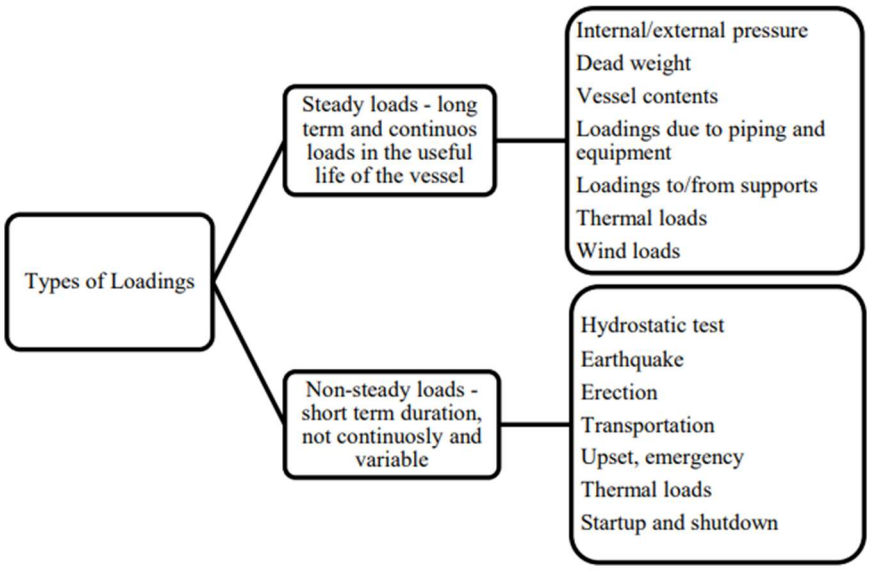

Figure 3: Categories of loadings based on frequency of application.

The characterization of a vessel involves specifying some of its characteristics, in particular:

- Operating Pressure: Maximum pressure expected during service.
- Design Pressure: Higher than operating pressure, with a safety margin.
- Operating Temperature: Maximum and minimum temperatures the vessel will encounter.

- Design Temperature: Corresponds to the design pressure, factoring in safety margins for temperature variations.
- Allowable Stress: Maximum stresses specified by the ASME Code to ensure safety.
- Corrosion Allowance: Additional thickness to counteract material thinning over time.

The design and construction of pressure vessels, given their danger in the event of rupture, are regulated by various design codes such as the ASME Boiler and Pressure Vessel Code in North America, the Pressure Equipment Directive (PED) in Europe, the Japanese Industrial Standard (JIS), and so on. *(Abdolreza, Tan Wai, 2019)*

Description of the pressure vessel used for the study

The vessel used for the study is provided by Baglioni S.p.A. It is classified under the products in the 'Inox Vessel' section, specifically in the vertical tanks subsection. The material is stainless steel AISI 304, and it undergoes pickling and passivation treatments. The fluids that can be contained are Group 2 fluids, which include compressed air, nitrogen, or a combination of compressed air and water (Fig. 4). It is designed following ASME VIII Div. 1 design code and approved in accordance with directive 2014/68/UE (PED). *(Baglioni Group, 2023)*

The technical drawing (Fig. 5) includes some identifying characteristics:

- Nominal Capacity 50 lt
- Design Pressure 11 bar at 120°C
- External Diameter 305 mm

Figure 4: Label on the Baglioni vessel.

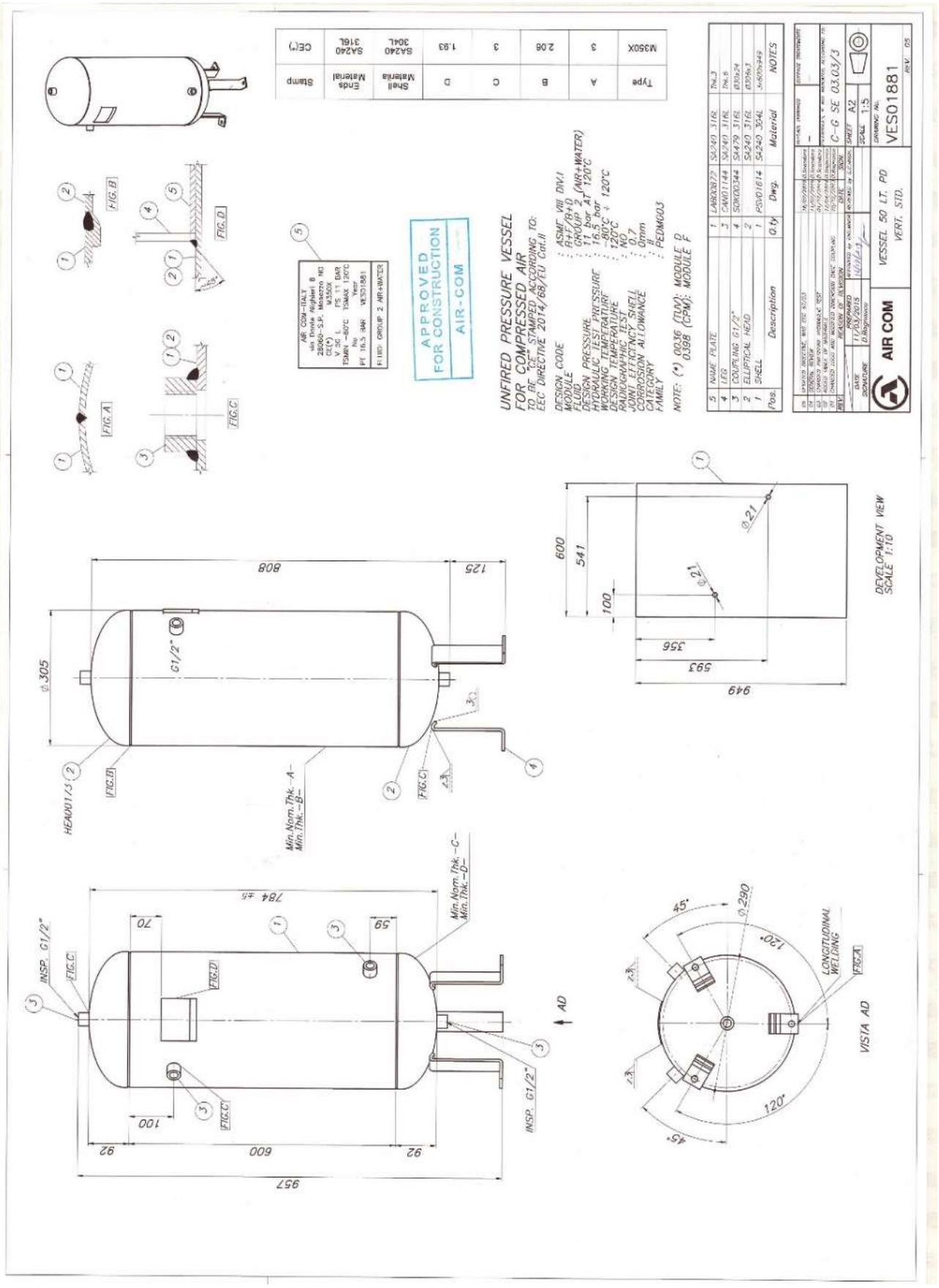

Figure 5: Technical drawing of the Baglioni vessel.

Calculation models

There is a dedicated theory that describes the stress and strain distribution through the thickness of the shell of reservoirs for high pressure fluids. This theory does not take into account edges or possible discontinuities for which it is necessary to use another approach. The theory describes two possible cases:

In this case we can exploit the hipotesis of thin walls because our vessel has a thickness of 3 mm and a diameter of 305 mm as we can see from the technical drawing (Fig. 6).

Figure 6: Difference between hipotesis of thin or thick walls.

For thin walls is set a cylindrical reference system r,θ,z (radial r, circumferential θ and axial z coordinate)and it is assumed that the circumferential stress $\sigma_{\theta\theta}$ is constant in the wall thickness. We can consider three different cases and, accordingly, three different versions of the Mariotte formula for circumferential and radial stress:

INTERNAL PRESSURE: $\sigma_{\theta\theta} = p_i \frac{r_i}{s}$ (1) $\sigma_{rr} = -p_i$ (2)

EXTERNAL PRESSURE: $\sigma_{\theta\theta} = p_e \frac{r_e}{s}$ (3) $\sigma_{rr} = -p_e$ (4)

INTERNAL AND EXTERNAL PRESSURE: $\sigma_{\theta\theta} = \frac{p_i r_i - p_e r_e}{s}$ (5) $\sigma_{rr} = p_i - p_e$ (6)

The axial stress can be assumed constant through the thickness but for boundary conditions we have to define what appens at the ends. There can be end edges blocked, end plates or free unloaded ends. For free unloaded ends axial strain is free and so the axial stress is null.

If there are end plates, as in this case (Fig. 7), calculating the equilibrium equation along axis direction we obtain:

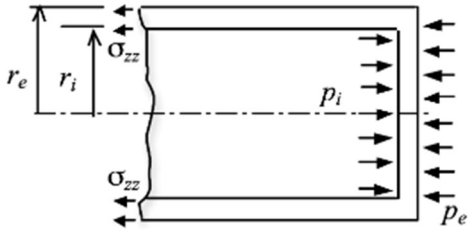

Figure 7: Stresses present in the presence of end plates.

$$\sigma_{zz} = \frac{p_i r_i^2 - p_e r_e^2}{r_e^2 - r_i^2} \quad (7)$$

In case of only internal or external pressure through simplifications you get:

$$\sigma_{zz} = \frac{\sigma_{\theta\theta}}{2} \quad (8)$$

To obtain the axial stress in the general form for end edges constrained we use the elasticity equation negleting the thermal expansion term:

$$\sigma_{zz} = v(\sigma_{\theta\theta} + \sigma_{rr}) = v\left(\frac{p_i r_i - p_e r_e}{s} + p_i - p_e\right) \quad (9)$$

The deformation is calculated by dividing the stress by the Young modulus E.The Baglioni vessel under study, like most pressure vessels, is manufactured using thin curved sheets and is axisymmetric. This allows for simple manufacturing processes and enhanced structural properties. Differently from plates shells can bear transverse loads by means of membrane stresses thanks to their curvature. Therefore, we can assume that stresses act in the mean surface and structure does not have load or structural discontinuities, except for the welds. The stress status can be described by superimposing two behaviours: membrane behaviour (stress and strain uniform in the thickness) and bending behaviour (stress and strane varying through the thickness). Under conditions of symmetric material, loads and constraints, the bending behaviour is significant only clolse to discontinuities and this is known as edge effect.

Due to small thickness, the shell can be studied considering the stresses on the mean surface and this makes particularly favorable the use of strain gauges as they are able to detect the deformation only on this surface.

This surface can be considered generated by the rotation of the meridian profile of the shell around the simmetry axis.

In axysimmetric shells stresses will be defined in a polar reference systems:

- meridian stress acting on cross section perpendicular to meridian direction σ_φ

- circumferential stress acting on the cross section perpendicular to parallel direction σ_θ

Accordingly we can define the meridian force per unit length n_φ assumed positive when outward and the cicumferential force per unit length n_θ. Shells can have various geometries for which the forces per unit length are calculated by imposing equilibrium; however, for this case study, only the cases of the cylinder and spherical cap are illustrated.

In a cylinder r_φ is infinite and $r_\theta = R$ and, imposing the axial equilibrium the meridian and circumferential force per unit length are obtained:

$$n_\varphi = \frac{P_o R}{2} \quad (10) \qquad n_\theta = P_o R \quad (11)$$

In a sphere $r_\varphi = r_\theta = R$ and it is possible to define a local coordinate $r = R \sin \varphi$ to be used for the equilibrium in axial direction (Fig. 8). We obtain constant forcers per unit length as in the cylinder but in this case they also have the same value.

$$n_\theta = n_\varphi = \frac{P_o R}{2} \quad (12)$$

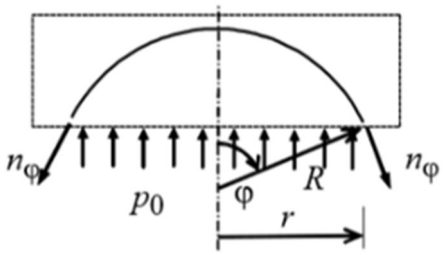

Figure 8: Stresses in the spherical shell

According to membrane theory, meridional n_φ and circumferential n_θ forces per unit length can balance the shell wall with respect to the internal pressure applied to the internal fluid. In transition areas between different shell parts and near constraints (like welds), membrane theory predicts discontinuities in forces per unit length. This leads to discontinuities in stresses and strains, and consequently to different displacements of connected shell edges. However, this is not actually possible as connected edges undergo the same displacements. The congruence in displacements is due to an additional stress state in the edges: thanks to these additional stresses, the displacements in different parts of the shell become equal and compatible.

It is possible to consider a connection between a cylinder and a semi-sphere as in our case, both with radius R, thickness s and undergoing internal pressure P. Due to the pressure the radius varies from R to (R + ΔR) and accordingly also the circumferential. The corresponding circumferential strain is calculated by means of the elasticity equation:

$$\varepsilon_\theta = \frac{\sigma_{\theta\theta}}{E} = \frac{n_\theta - \nu n_\varphi}{Es} = \frac{P_o R}{2s} \quad (13)$$

Substituting in this the expressions of the corresponding membrane forces per unit length we find different radius variation that will be offset by the additional edge stress:

$$\Delta R_{sphere} = \frac{P_o R^2}{2Es}(1-\nu) \ (14) \ \Delta R_{cylinder} = \frac{P_o R^2}{2Es}(2-\nu) \ (15)$$

The solution of this problem involves local stresses, meaning that the stress distribution due to edge effects ends at short distances from the edges, furthermore edge stresses are self-equilibrating because the pressure is already balanced by membrane stresses. Therefore, if the edge stresses reach the elastic limit, local plasticization of the vessel occurs. This plasticization does not lead to collapse, unlike membrane stresses caused by internal pressure. The membrane stresses are referred to as primary stresses, while the edge stresses are referred to as secondary stresses.

On the cross-sectional surfaces perpendicular to the cylinder's axis, there are also shear stress components that are radially directed. These are not considered in the resistance behavior but are accounted for in the equilibrium equations of the elementary element, considering the shear force per unit length they generate.

Regarding the local effects, if an infinitesimal element of the shell is considered, it is not necessary to take the fluid pressure into account because it is balanced by the general stresses. The load per unit area coincides with the effect of the local membrane circumferential stress because the bending moment per unit length is not considered in the equilibrium. By utilizing the equilibrium equation in the radial direction and the equilibrium of rotation, it is found that the shear stress in the infinitesimal unit is the derivative of the bending moment with respect to the coordinate. The edge stresses are thus maximal at the edges and zero far from these points.

The stresses can be divided into primary and secondary. The primary ones are those that balance the internal pressure, while the secondary ones are local, such as the edge effects. These are responsible for deformations that ensure congruence and can exceed the elastic limit without interfering with equilibrium. *(Sesana, 2023)*

Calculation of stresses on the Baglioni vessel

The calculations on the Baglioni vessel are carried out according to the thin-walled vessel model using the formulas explained previously and taking into account the rigidity through the Poisson's ratio coefficient v. The calculated stresses are presented in (Tab. 2) and expressed in MPa, while the deformations are represented by dimensionless numbers.

ri	149,5	mm
s	3	mm
E	192000	

Table 1: Data used for stress calculation.

P (bar)	σθθ (MPa)	σzz (MPa)	εθ	εz
1	4,983333333	2,491666667	2,36189E-05	1,18E-05
2	9,966666667	4,983333333	4,72378E-05	2,36E-05
3	14,95	7,475	7,08568E-05	3,54E-05
4	19,93333333	9,966666667	9,44757E-05	4,72E-05
5	24,91666667	12,45833333	0,000118095	5,9E-05
6	29,9	14,95	0,000141714	7,09E-05

Table 2: Results of stress calculation.

FEA simulation of the Baglioni vessel and calculation of stresses and deformations

Finite Element Analysis (FEA) is a numerical technique used to solve complex engineering problems involving structures, fluids, heat transfer, electromagnetism, and other fields. FEA divides a complex model into small and simple parts called finite elements, which collectively form a mesh. This mesh is composed of nodes that provide the basis for approximating the differential equations governing the physical behavior of the system.

This analysis process involves several steps:

1. Model Creation: Creation of a geometric model of the system or structure to be analyzed. This model can be either two-dimensional or three-dimensional, depending on the problem.
2. Assignment of Material Properties: Material properties, such as elasticity modulus, density, and thermal conductivity, are assigned to each element of the model.
3. Discretization (Mesh Generation): The geometry of the model is divided into a series of finite elements. The quality of the mesh, meaning the size and shape of the elements, directly affects the accuracy and efficiency of the analysis.
4. Application of Loads and Boundary Conditions: External loads, forces, pressures, or temperatures are then applied, and boundary conditions are imposed, representing the constraints or interactions of the system with its external environment.
5. Equation Solving: Using numerical methods, the software solves the differential equations governing the behavior of the finite elements, determining variables such as deformations, stresses, temperatures, and flows.
6. Post-Processing: The obtained results are visualized and analyzed through graphs, color contours, or animations to interpret the model's behavior.

ANSYS is one of the most advanced and widely used software for finite element analysis. Created by ANSYS Inc., it offers tools for structural, fluid dynamic, thermal, and electromagnetic analysis. The software is modular, with each module specifically designed for particular types of analysis, such as ANSYS Mechanical for structural analysis, ANSYS Fluent for computational fluid dynamics, and ANSYS Maxwell for electromagnetic analysis. In the case study at hand, the ANSYS Mechanical module

will be used. Thanks to its sophisticated solution technology and optimization capabilities, ANSYS is known for the accuracy and reliability of its results, often verified and validated by industry experts. However, in this case, ANSYS Student is being used, which is a free version of the software for students. It has all the necessary features for conducting a finite element analysis but limits the number of mesh nodes, ensuring that the mesh is not too fine, thereby slightly reducing accuracy.
After this brief introduction, the previously described steps are used to outline the study of the Baglioni vessel.

Model Creation

To create the project, the ANSYS Workbench module is used. It requires several initial specifications, such as the geometry of the body and the type of analysis to be performed. Regarding the body's geometry, Baglioni provides the 3D model of the vessel, but some modifications are necessary to make it suitable for use in ANSYS. For this purpose, the .igs file of the body assembly was exported and imported into the 'Geometry' section of the project. At this point, using the ANSYS Discovery module, the various parts of the vessel are combined to form the main rigid bodies: upper and lower heads, shell, support legs, nozzles, and the nameplate with the vessel details. Another necessary modification is the physical union of the legs to the lower head to properly simulate their contact. Then, the sizes are verified to ensure they match those indicated in the drawing (Fig. 5). Once the geometry is entirely correct (Fig. 9), returning to the Workbench module, the type of analysis to be performed is selected: in this case, a static structural analysis. At this point, the 'Model' section linked to the ANSYS Mechanical module can be opened.

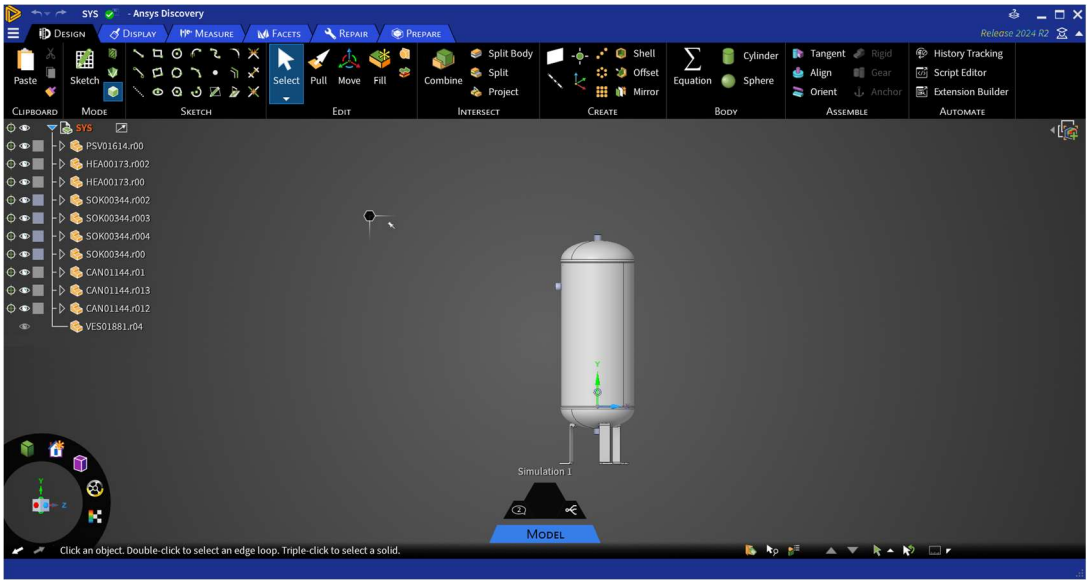

Figure 9: Geometry of the body.

Assignment of Material Properties

Once the model is opened and it is confirmed that the geometry has been correctly loaded, the next step is to assign the material properties to the various bodies. However, before this can be done, the materials need to be specified in the Workbench under the "Engineering Data' section. Here, you must search the various libraries to see if the desired material is available, or, as in this case, create a new personal library and add a material with the desired specifications (Fig. 10). Once this is done, the model needs to be updated, and then the material can be assigned to the various bodies.

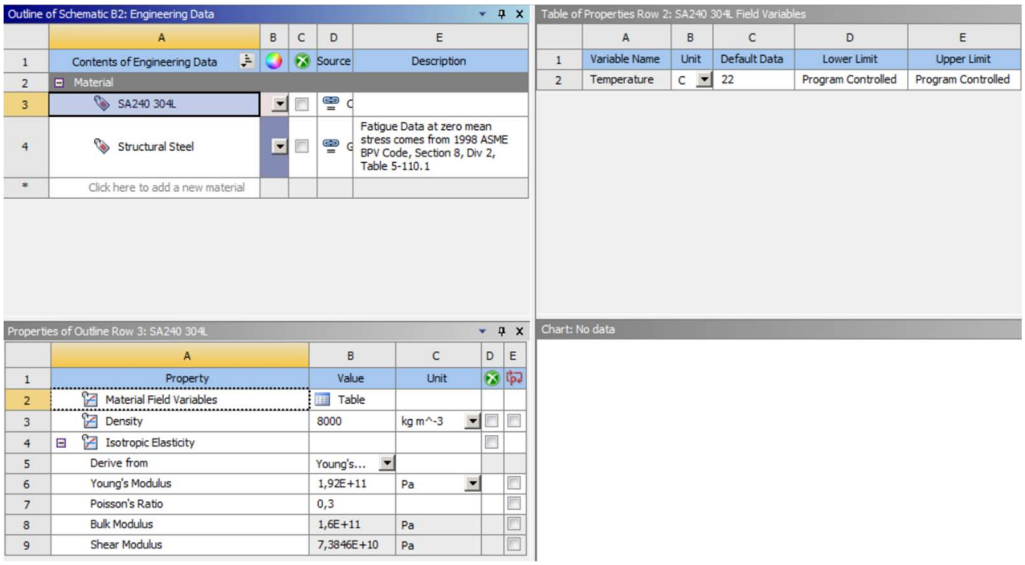

Figure 10: Definition of the material.

Discretization (Mesh Generation)

As previously mentioned, mesh definition is subject to certain limitations in ANSYS Student. Various attempts are made to assign element sizes to determine the one that allows for the finest possible mesh without causing licensing issues. After several trials, a size of 1.5 cm is determined (Fig. 11). If there were no limitations, the ideal solution would be to create meshes of different sizes based on the dimensions of the bodies and the desired level of accuracy for each of them (for bodies where uniform results are expected, a less fine mesh is still acceptable). However, in this case, it is important to ensure that the contact surfaces between the different meshes do not cause issues, using the merge command between them.

Figure 11: Results of the meshing phase.

Application of Loads and Boundary Conditions

Before proceeding with the application of constraints and loads, it can be useful to check the contact surfaces between the various bodies in the 'Connections' section. It is important to ensure that all contact surfaces are indicated and that each one has the correct type of contact specified, which in this case is always 'Bonded' because it best simulates welds (Fig. 12).

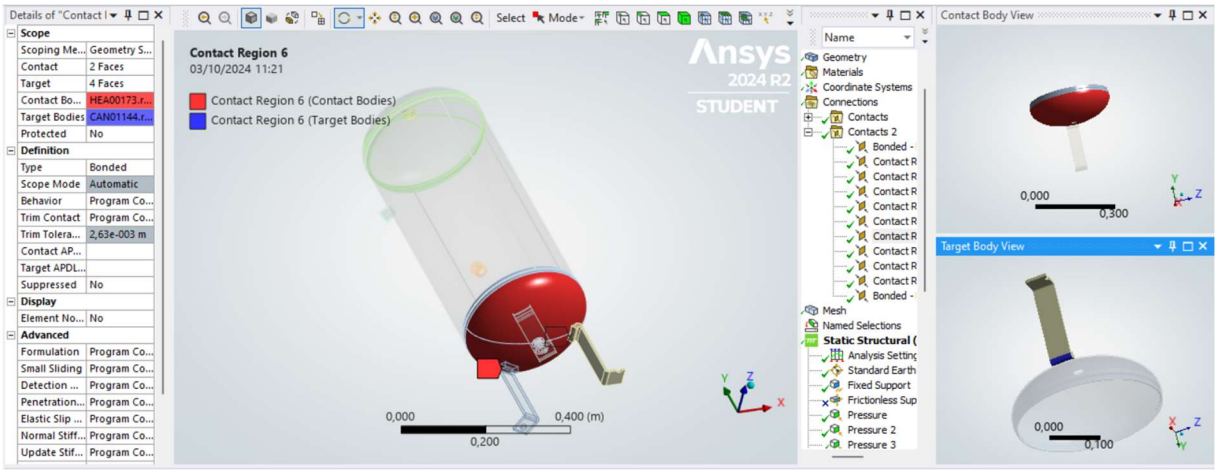

Figure 12: Example of a connection definition.

By specifying the boundary conditions, the goal is to replicate the conditions under which the tests on the vessel will be conducted. For this purpose, in ANSYS, the gravitational acceleration effect (i.e., the weight of the bodies) is applied from the Static Structural library, the ground support for the feet is defined as 'Fixed Support' and finally, a 'Displacement' constraint with zero degrees of freedom in all directions is imposed on the various nozzles to simulate their closure (Fig. 13).

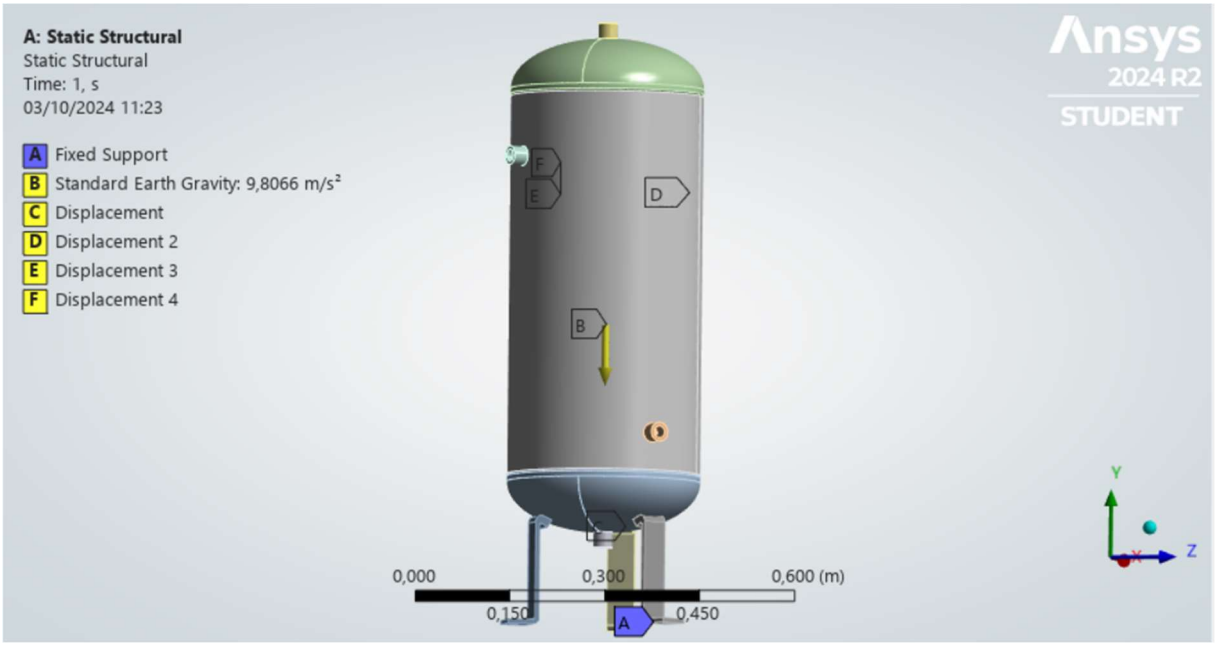

Figure 13: Boundary conditions applied.

The vessel will be pressurized, so the loading conditions can be replicated by applying pressures of the same intensity on the internal surfaces of the vessel, acting in the normal direction and as surface effects (Fig. 14).

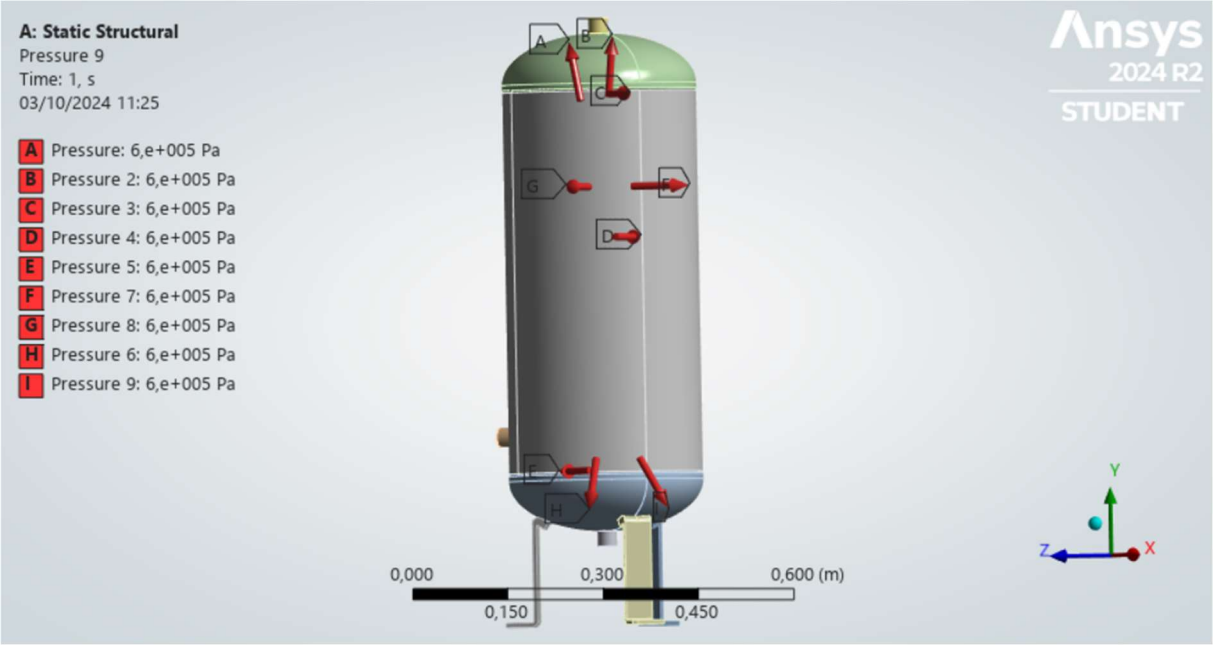

Figure 14: Pressure applied.

Post-Processing

Once all the previous steps are completed, the simulation can be started to obtain results by pressing the 'Solve' command. However, before doing so, it is necessary to specify in the 'Solution' section which results you want to visualize. In this case, directional deformations are of interest, for which a new cylindrical coordinate system must be created, as the focus is on axial and circumferential deformations. It is also possible to view stresses, stress states, total deformations, energy states, and so on.

Results of FEA and comparison with analytical stresses.

Finite Element Analysis (FEA) and theoretical formulas are both effective methods for evaluating the performance of thin-walled vessels, but they can yield different results for various reasons, such as the different limitations and assumptions inherent in each method. In this case, the deformations calculated using theoretical formulas and those obtained through FEA differ by about a multiplication factor of 10. The possible reasons for this discrepancy are then listed and described.

Firstly, Mariotte's formulas for thin-walled vessels are based on some simplifying assumptions, such as:

- Uniform Material Properties (Isotropy):It is assumed that material properties are uniform and constant throughout the body and in all directions.

- Perfect Geometry: The geometry is assumed to be ideal, neglecting imperfections or deviations from the theoretical shape.
- Simplified Loading Conditions: The loading conditions are assumed to be uniform or simplified, not always reflecting real variations.

FEA, on the other hand, models the geometry and material properties more accurately and can account for complex loading conditions. Due to the more detailed nature of the analysis, its results can differ from theoretical predictions.

The quality of the mesh also influences the results obtained from FEA simulations: a finer mesh can provide more accurate results by capturing more detailed variations in stress and deformation. However, this also increases computational effort. If the mesh is too coarse, it might not capture critical details, leading to less accurate results.

The type of elements used in the mesh (e.g., triangular, quadrilateral, hexahedral) can also affect the results, as some elements may be better suited to specific types of problems. Theoretical formulas do not consider such mesh details, as they are based on continuous and idealized models rather than discrete numerical approximations.

The application of boundary conditions and loads in FEA can differ significantly from those assumed in theoretical formulas: in softwares, boundary conditions can be applied with high precision, including constraints and complex interactions between different parts of the model (in this case, for example, ground support and various welds). Theoretical formulas can only assume simplified boundary conditions. FEA allows the application of complex and non-uniform loads, which is not possible with theoretical formulas.

Theoretical formulas for thin-walled vessels are often derived assuming linear elastic behavior. They may not consider:

- Material Nonlinearity: Real materials can exhibit nonlinear behavior under certain conditions, such as plastic deformation or viscoelastic effects, which theoretical formulas might not take into account.
- Complex Loading Conditions: FEA can incorporate various types of nonlinearity, such as large deformations or material plasticity, which are typically beyond the scope of simple theoretical formulas.

Therefore, FEA results may reflect a more realistic behavior of the material and loading conditions.

Despite the greater accuracy of the results obtained with FEA compared to theoretical formulas, it is necessary for this model to be validated and calibrated using experimental data to identify discrepancies and refine the model.

Below are the FEA results represented graphically on the 3D model of the vessel. The axial deformations (Fig. 15), circumferential deformations (Fig. 16), and total deformations (Fig. 17) are shown. The values are lower than those theoretically predicted, but as explained in this chapter, this is due to the differing accuracy of the simulation.

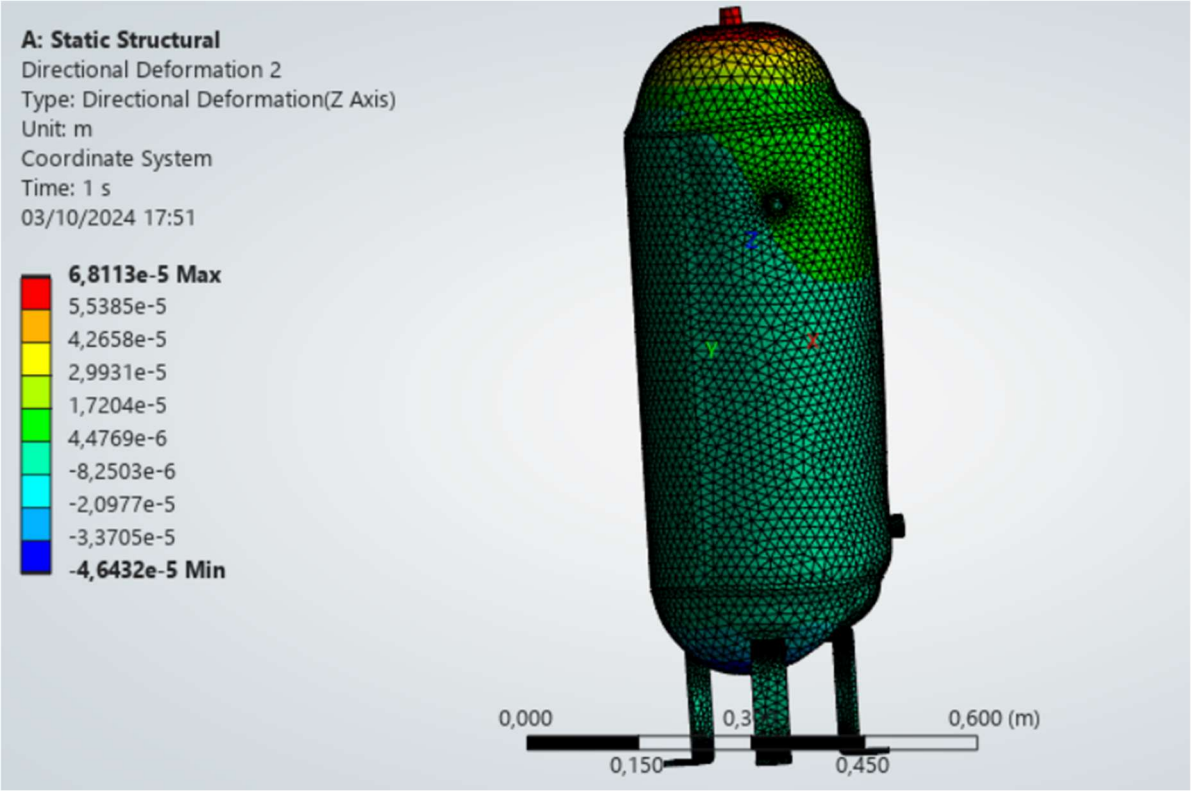

Figure 15: Results: axial deformations.

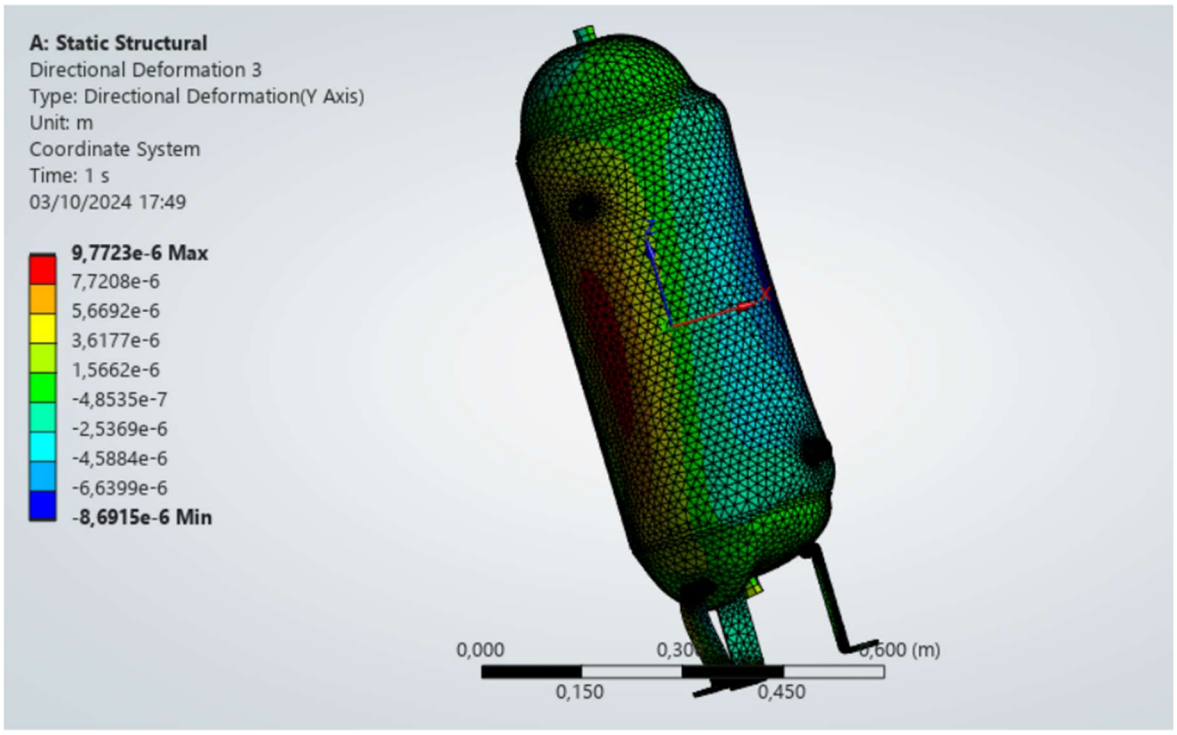

Figure 16: Results: circumferential deformations.

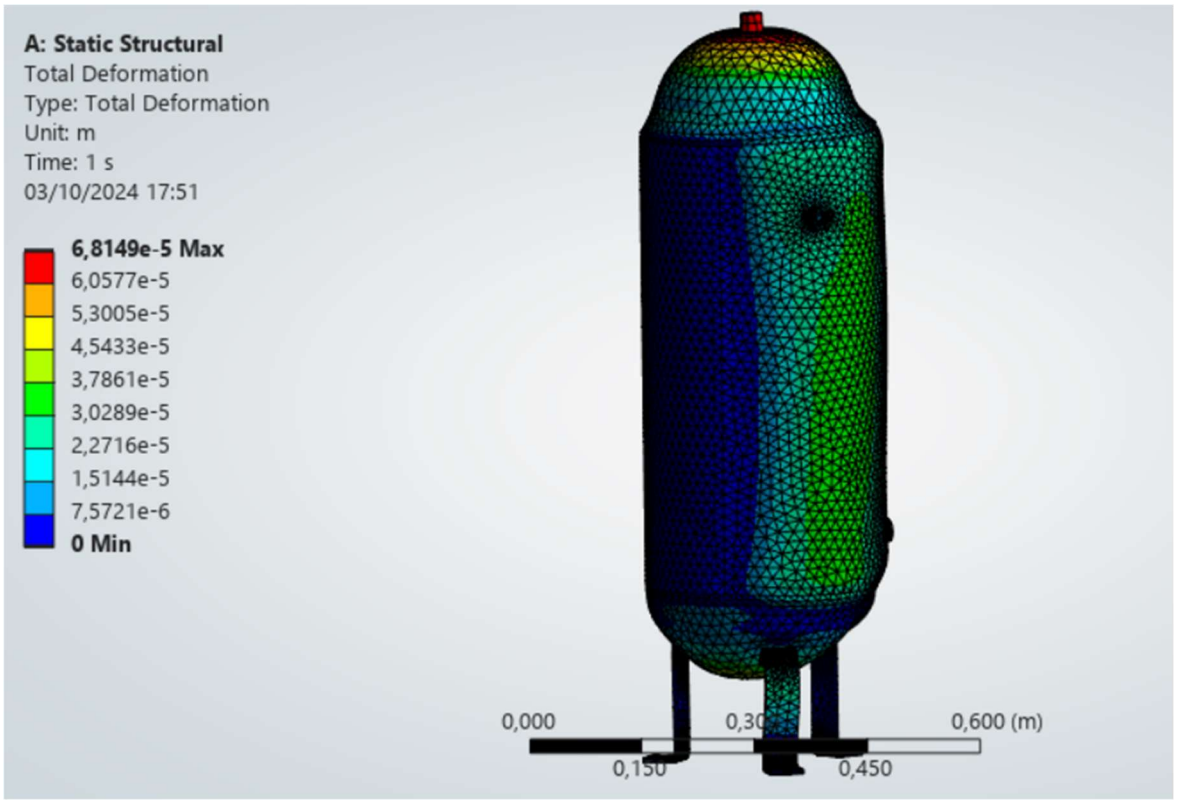

Figure 17: Results: total deformations.

Experimental strain measurement

Introduction on strain gauges

The experimental phase of data acquisition is carried out using devices called electrical strain gauges. Strain gauges are measuring instruments that exploit the deformations of the body to which they are attached, typically subjected to mechanical or thermal stresses. They are capable of measuring the distance between two points of the test element and, consequently, the deformation defined as:

$$\varepsilon = \frac{\Delta l}{l} \quad (16)$$

By knowing the specific characteristics of the material, it is possible to determine the loads to which it is subjected. With correct placement of the strain gauges, it is also possible to understand the direction and magnitude of these loads.

These devices must be characterized by a calibration constant (gauge factor) (that should remain constant under various conditions), should have a relatively low cost, and be capable of accurately measuring local deformations.

The deformation is usually so small that direct measurement is not possible. In this case, electrical strain gauges are used. These consist of a grid of thin metal wire that follows the deformations of the surface to which it is attached, changing its electrical resistance (Fig. 18). The sizes can vary, but smaller devices are typically used for point measurements. It is also possible to use rosettes, which are bases with multiple strain gauges placed in different directions. The change in resistance is instantaneous, allowing observation of both static and dynamic deformations at high frequencies.

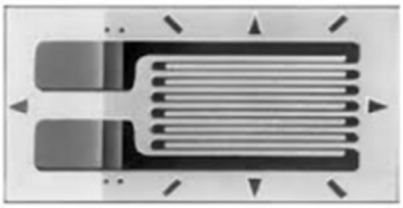

Figure 18: General scheme of a strain gauge.

As is well known, electrical resistance depends on the resistivity of the material, the length of the conductor, and the area of its cross-section according to the formula:

$$R = \frac{\rho l}{A} \quad (17)$$

Differentiating and dividing by R :

$$\frac{\Delta R}{R} = \frac{\Delta \rho}{\rho} + \frac{\Delta l}{l} - \frac{\Delta A}{A} \quad (18)$$

Considering the longitudinal deformation ε_l and the resulting transverse deformation caused by a uniaxial stress state: $\varepsilon_t = -v\varepsilon_l$

$$\frac{\Delta R}{R} = \frac{\Delta \rho}{\rho} + (1 + 2v)\varepsilon_l \quad (19)$$

This highlights the relationship between the relative change in resistance and the longitudinal deformation.

In this way, the deformation of the body will be the same as that of the strain gauge and thus measurable by the change in resistance. Typical resistance values are 120Ω or 350Ω with tolerances of 1%.

The gauge factor indicates the sensitivity of the strain gauge and is calculated as:

$$G = \frac{\frac{\Delta R}{R}}{\frac{\Delta L}{L}} \quad (20)$$

That is, the relative change in resistance divided by the deformation. A typical sensitivity value is G = 2, with tolerances between 1% and 2%.

Strain gauges are also sensitive to temperature variations, making it important to monitor these changes. It is also necessary to consider that at high temperatures, the adhesive might lose its effectiveness, and the materials of the grid and wiring might get damaged.

Measurement errors due to temperature variations can be avoided by using self-compensating strain gauges or external compensation methods. This is crucial because electrical resistance is influenced by temperature according to the relationship:

$$\left(\frac{\Delta R}{R}\right)_{\Delta T} = \alpha \Delta T \quad (21)$$

Additionally, temperature causes different thermal expansions between the material of the piece and that of the strain gauge, generating an apparent deformation.

As mentioned earlier, one way to avoid problems due to variable temperature is to use a compensating strain gauge connected in a half-bridge configuration with the measuring gauge. In this way, the effects they experience are canceled out by being

on the same side of the Wheatstone bridge (Fig. 19). *(Ortombrina, 2013) (Gobbi, 2012) (Cazzato, 2018) (Bonfanti, 2020)*

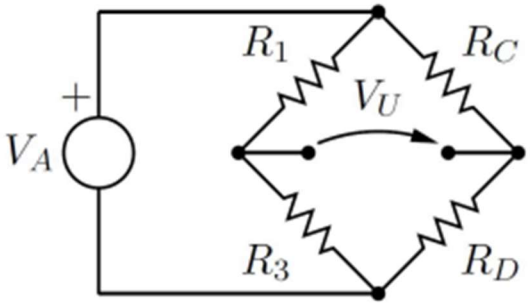

Figure 19: The Wheatstone bridge in a half-bridge configuration with two fixed strain gauges, one for measurement and one for compensation.

Figure 20: Technical data sheet of the strain gauges used. (HBM, n.d.)

Installation of strain gauges on vessel and verification of operation

The bonding phase is critical because if this step is not performed correctly, the quality of the measurement suffers since the sensor must experience exactly the same deformation. The strain gauge is attached to the body by first lightly sanding the surface to create some roughness, followed by cleaning to remove impurities. Then, it is bonded using suitable adhesives, with the right amount: too little will not adhere well to the sensor, while too much will create a disturbing elastic layer. Although the

sensitive area is only the one covered by the grid, it is important to ensure that the entire polymer base is well bonded and does not overlap with other sensors.

The strain gauge is positioned in axial and circumferential directions at strategic points. Marks are made on the piece for alignment, which is ensured by using tape during both positioning and bonding. Along with it, pads are installed for soldering the sensor's incorporated wires, ensuring that the necessary soldering for data transmission does not occur on the device body but on a separate support body.

In our case, the fixed strain gauges and the temperature compensating strain gauges are placed at various points on the vessel. Some of them are not affected by any particular effect, while others are positioned at the circumferential and axial welds, at the point where they intersect, around the base of the nozzle to observe the effect of the welds at close range. Four pairs of sensors are also placed on the lower spherical cap, them could be placed in any position since the stresses here are equal in all directions.

Each strain gauge is identified by a code. In the first rows of the table, we find the strain gauges on the side of the container. Their codes consist of a number (indicating the height at which they are placed), a first letter indicating the installation direction, and a third letter differentiating the two strain gauges paired in the same direction (Fig. 21 and 22). Subsequently, the strain gauges around the nozzle (Fig. 23) are identified with an initial number 4, a letter indicating the direction, and four different letters for the 4 pairs. Finally, the strain gauges on the bottom dome are grouped into group 6 and differentiated not by direction (which is irrelevant in this case) but by a method to identify the 4 pairs (Fig. 24).

1CA	1CB
1AA	1AB
2CA	2CB
2AA	2AB
3CA	3CB
3AA	3AB
4AA	4CA
4AB	4CB
4AC	4CC
4AD	4CD
6A	6C
6B	6D

Table 3: Codes of the strain gauges.

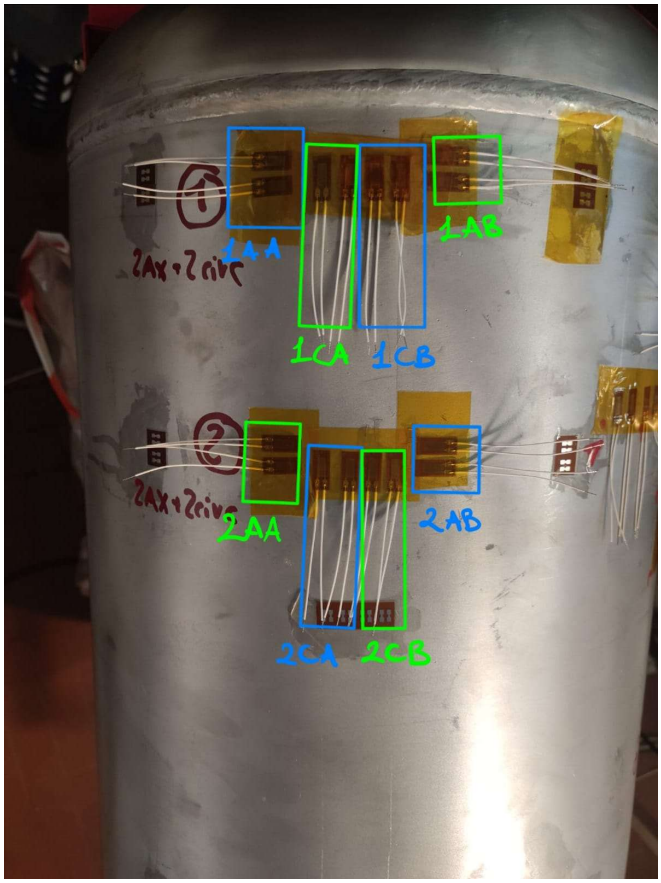

Figure 21: Strain gauges on the side of the container 1.

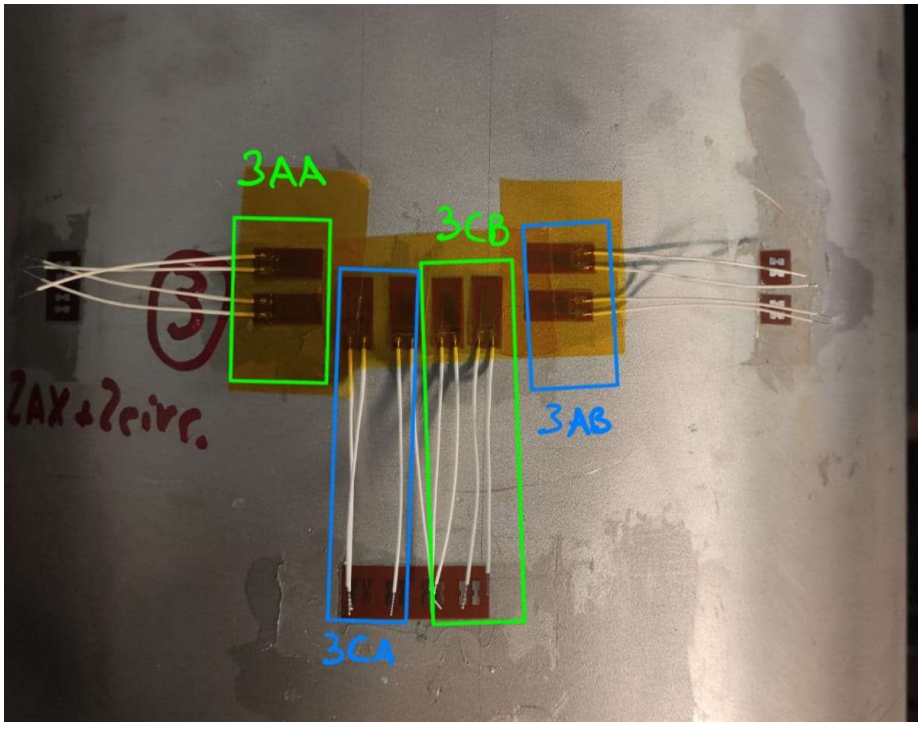

Figure 22: Strain gauges on the side of the container 2.

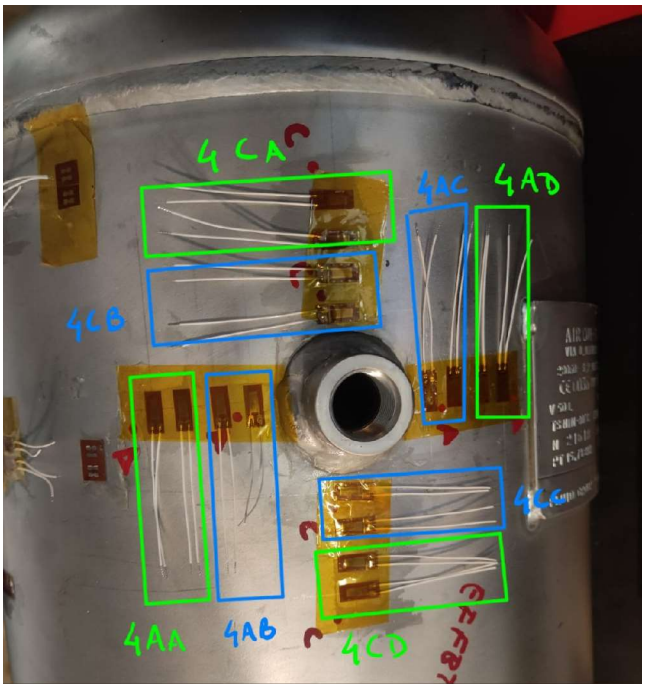

Figure 23: Strain gauges around the nozzle.

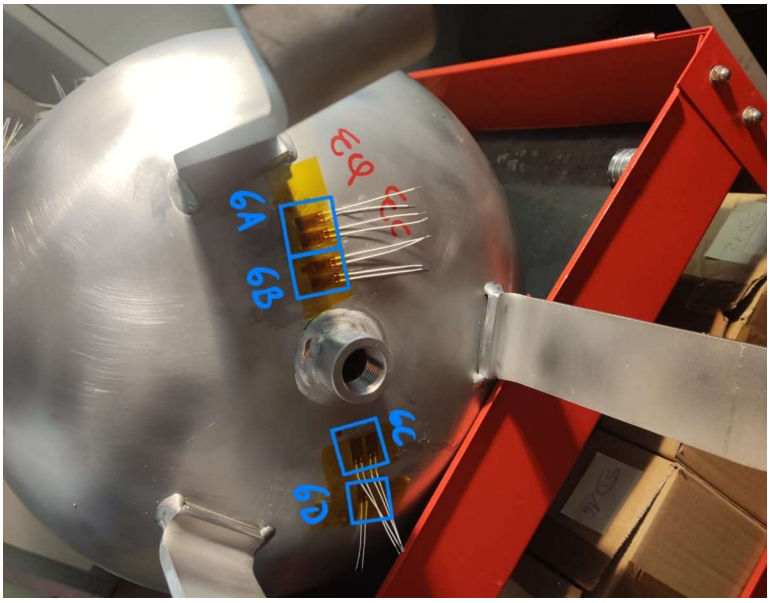

Figure 24: Strain gauges on the bottom dome.

The temperature compensating strain gauges are positioned next to the fixed ones without adhesive but using tape, and the half-bridge connection is made by soldering the wires together on the pads (Fig. 25).

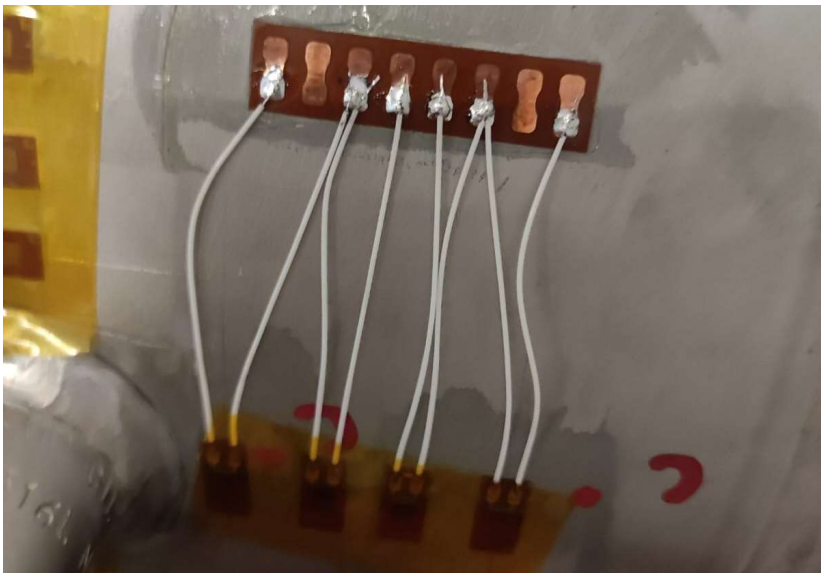

Figure 25: Wires soldered on the pad.

The correct execution of the solder joints is verified using a multimeter: the terminals are placed on the solder joints made with the tin wire between the strain gauge tabs and the support pads. The solder joints are compared in pairs, with two pairs composed of a single tab on one side and central joined tabs, and one pair formed by the two outer single tabs. When measuring the first two pairs, if the connection is functional, the exact resistance value of the strain gauges will be observed on the multimeter screen, while for the last pair, the observed value will be double, as it creates a series connection. The solder joints that do not return these values are corrected and tested again until they function properly.

Subsequently, the insulated cable necessary for connection to the acquisition board is soldered with tin. It consists of an outer protective insulating layer and inside, four mono-cables distinguished by different colors. In the case study in question, only three cables will be used (Fig. 26): the red one will be connected to the bridged tabs, while the green and blue ones will be connected to the outer tabs. The last cable (yellow) will be cut later to avoid errors and for convenience during the connection phase to the acquisition board. The correct soldering of the insulated cable is also verified using the multimeter.

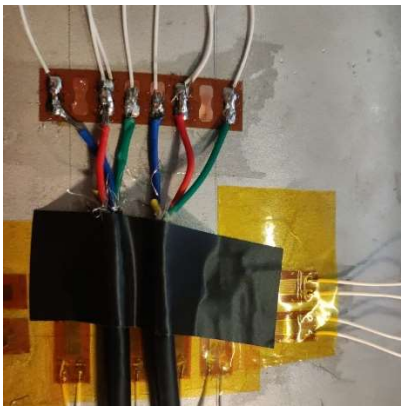

Figure 26: Insulated cable soldered on the pad.

Connecting Strain Gauges to the Acquisition System and Verifying Functionality

The acquisition system (DAQ) used is the QuantumX MX1615B strain gauge amplifier produced by HBM. The instrument manual provides details on all possible connection types and their respective configurations. In this specific case study, the connection is a half-bridge type with three main cables (Fig. 27).

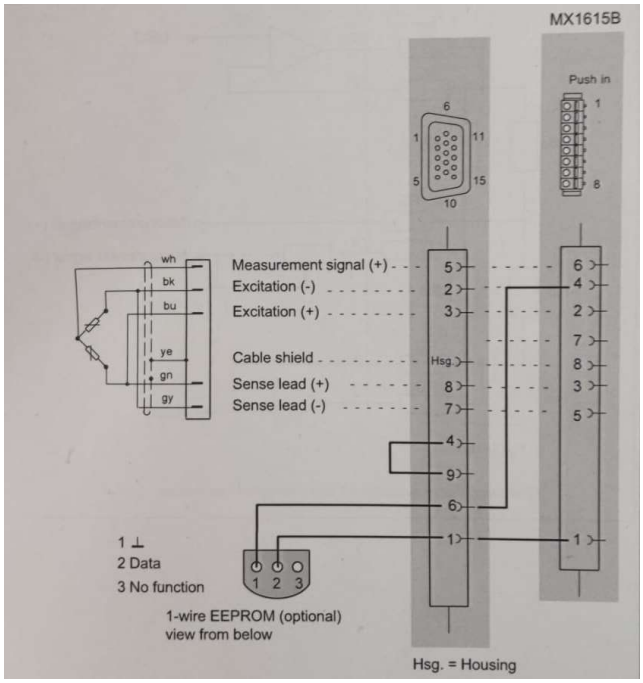

Figure 27: Wiring diagram for the half-bridge connection.

The correct connection to the amplifier is indicated by the green LED associated with the acquisition channel (Fig. 28).

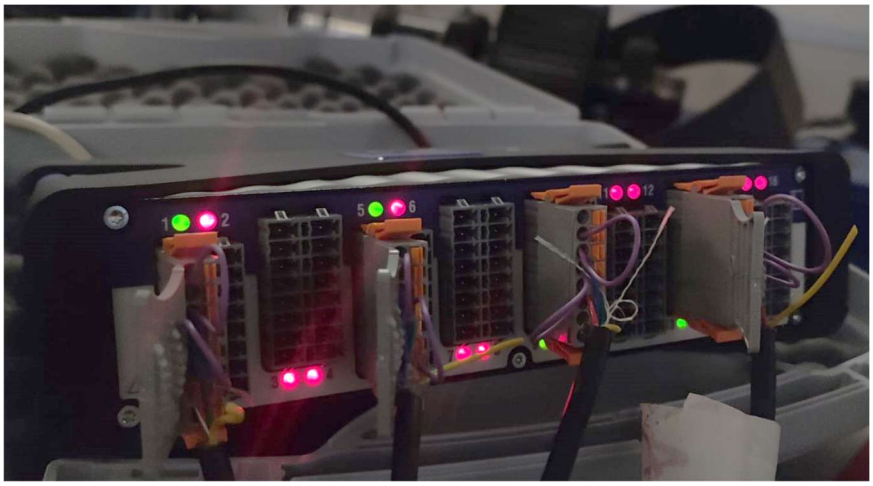

Figure 28: Connection to the HBM acquisition board.

For data visualization, the HBM CatmanEasy software is used. By specifying the cable configuration associated with each channel and the desired acquisition frequency, the software allows real-time observation of the selected variable. Additionally, without the need for other software, the program can run to produce a graph of the data trends for the selected channels and, upon completion, export the dataset in various formats.
In this case study, a half-bridge connection was associated with the four channels used, with a 'slow' acquisition frequency (10 Hz). The data were exported from the DataViewer section, already processed (Min, Max, Mean, and STD), and tabulated in an Excel file. *(HBM, n.d.)*

Test Execution: Pressurizing the Container at Different Pressure Levels, Verifying Linearity and Hysteresis, Comparing Experimental and Calculated Strains

To perform the tests, it is necessary to install various hydraulic components on the vessel, namely the pressure gauge at the top for pressure monitoring (Fig. 29) and three valves at the base one for connecting to the pump for the pressurization phase, one for emptying and filling, and one connected to the small pipe for reading the water level (Fig. 30).

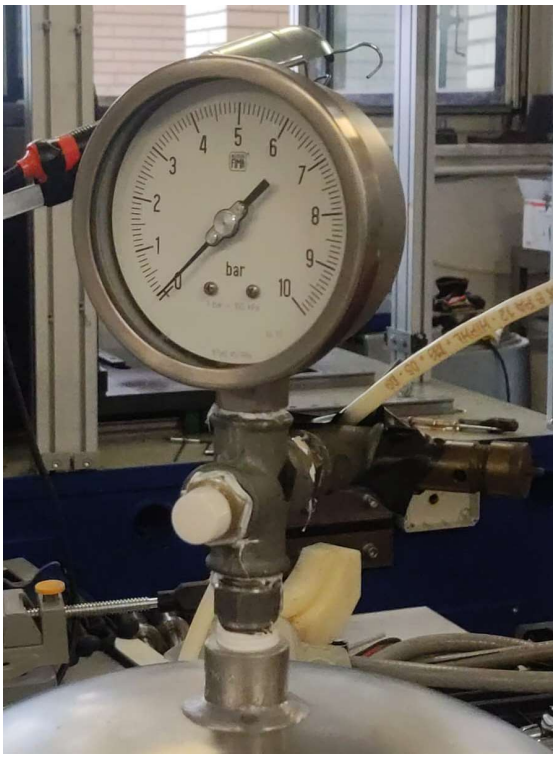

Figure 29: Pressure gauge installed.

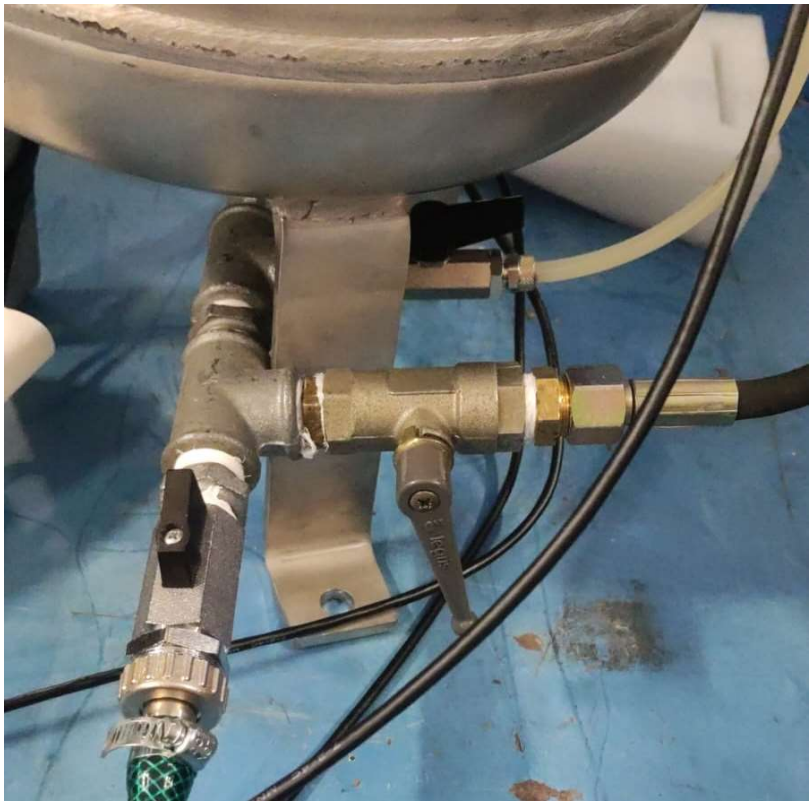

Figure 30: Valves installed at the base.

Once this operation is completed, proceed to fill the container to a level slightly above the circumferential weld. This step takes longer than expected as it requires simultaneous release of the air inside through a small vent valve located below the pressure gauge as water enters.

With the container filled, electrical connections are made between the strain gauges and the acquisition board, which is then connected to a computer with Catman software license via an ethernet cable. It is necessary to verify that the channels in use are functioning correctly, adjust the initial settings mentioned earlier, and immediately before starting the acquisition, zero the reading to ensure data accuracy and reliability. In this case, a slow acquisition frequency is chosen, the half-bridge configuration is set, and strain is measured.

At this point, pressurization of the container can begin. In this case, this was done by manually pumping water into the container and checking the pressure increase with the pressure gauge. Each time the pressure inside the container increases by 1 bar, a run is performed on the software for about 10 seconds. This is because the values oscillate slightly around a mean value, and within this specific time interval, approximately 100 samples are recorded, allowing the program to calculate the maximum, minimum, mean, and standard deviation (STD) values, which will then be used in Excel for interpretation.

This operation is repeated at 1 bar intervals from the initial 0 bar up to 6 bar. At this point, the pressure is reduced again, following the same steps, using the aforementioned vent valve. These data are also recorded to confirm or refute the occurrence of a hysteresis phenomenon.

Hysteresis in the deformations of a material subjected to loading and unloading cycles refers to the tendency of the material not to follow the same deformation path during the positive and negative phases. This phenomenon is graphically manifested as a hysteresis loop when plotting the stress-strain curve. For metals in particular, after a complete cycle of loading and unloading, the material may not return exactly to its original configuration. This permanent deformation is known as residual plastic deformation.

Results and Graphs

The results of the experimental phase are represented by plotting the stress-pressure curves for both the loading and unloading phases to visualize the hysteresis loops. Additionally, for each cycle, the R^2 index is reported, indicating the deviation of the deformation from the linear trend: a value closer to 1 indicates a smaller deviation, and thus a greater amplitude of the hysteresis loop.

Some strain gauges show fewer cycles due to errors caused by cable movements during the test. Additionally, for two strain gauges, no results are reported due to damage that prevents their operation. This lack of data is not a problem because, as it is possible to observe from the figures 31 to 48, for each pair of strain gauges, an equivalent mirrored pair is provided.

The results obtained by the strain gauges on the lower shell will be analysed separately in the next chapter.

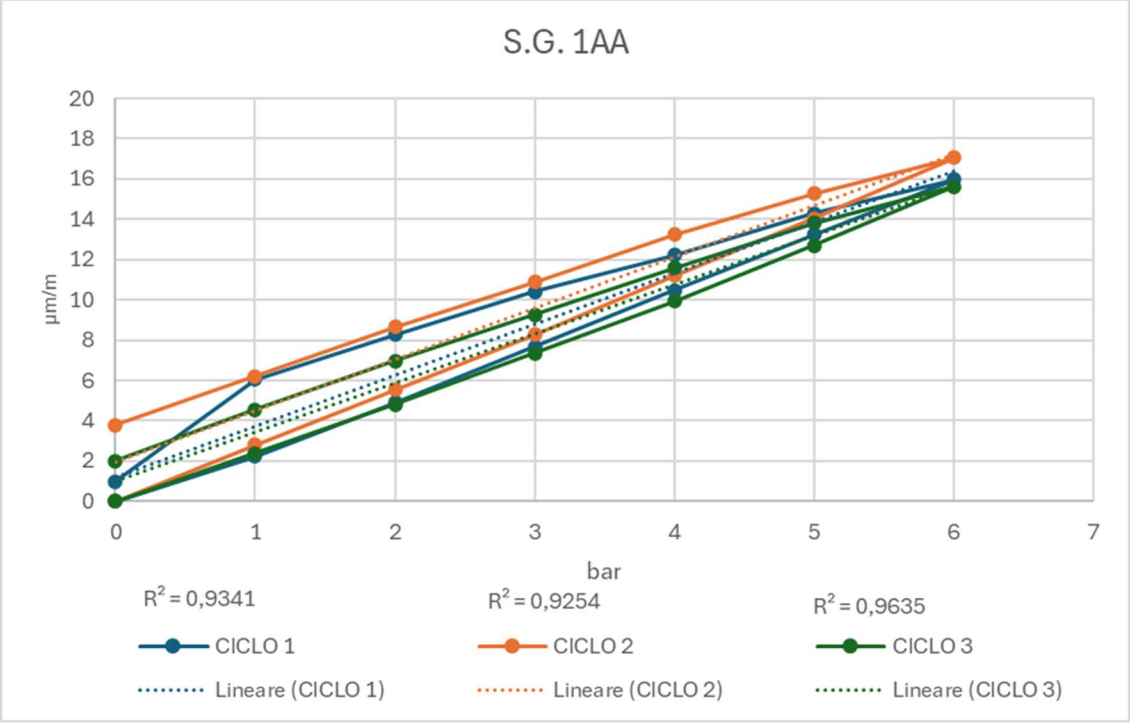

Figure 31: 1AA strain gauge results - axial.

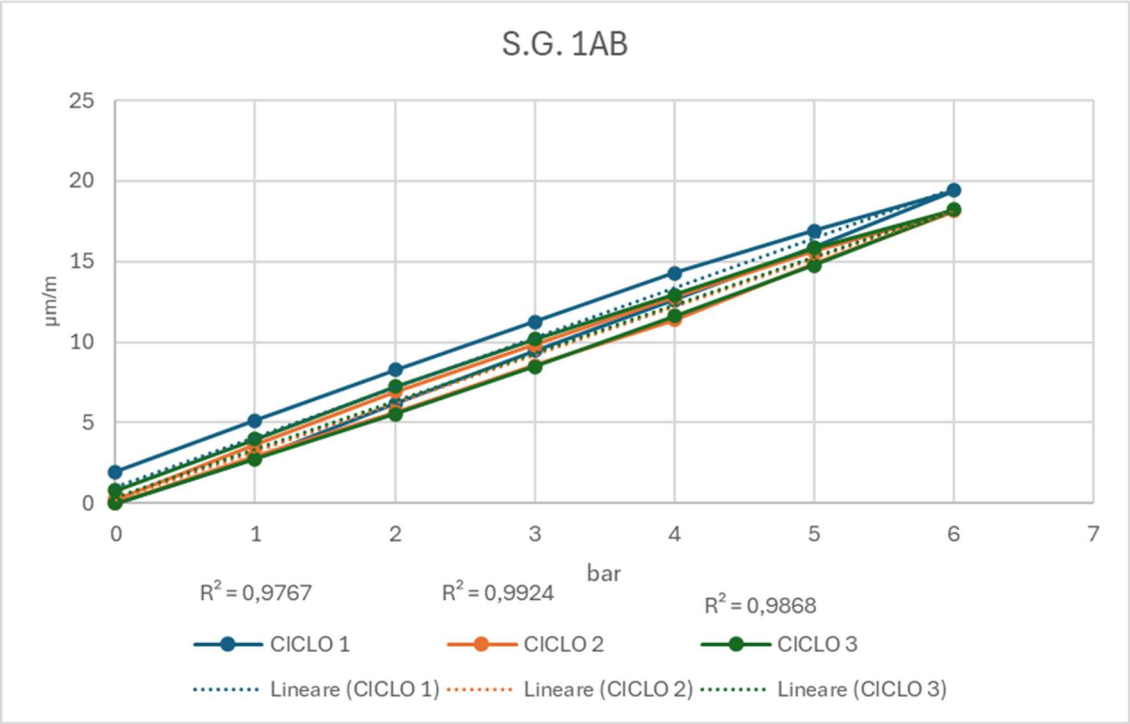

Figure 32: 1AB strain gauge results - axial

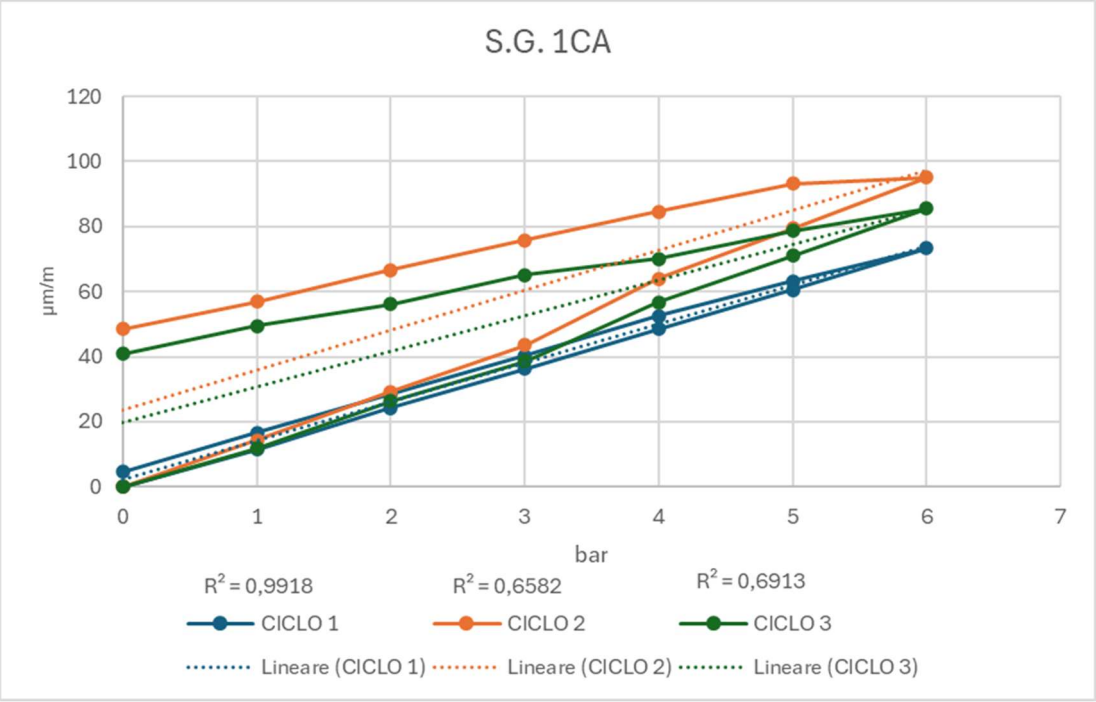

Figure 33: 1CA strain gauge results - circumferential.

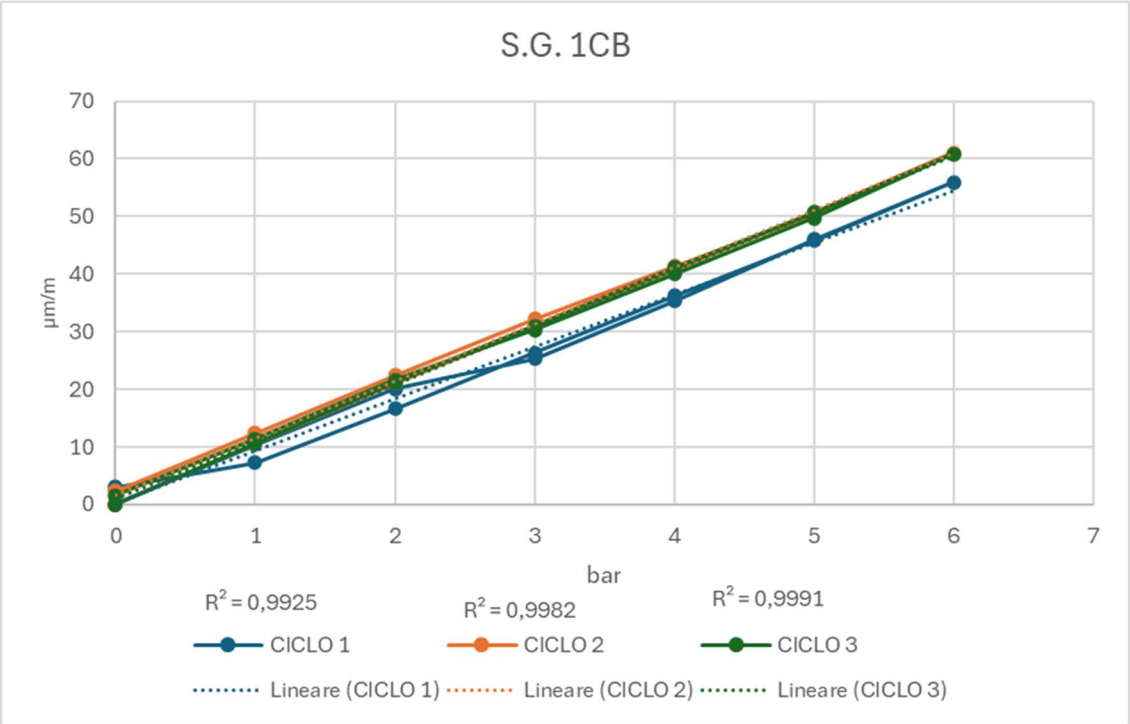

Figure 34: 1CB strain gauge results - circumferential.

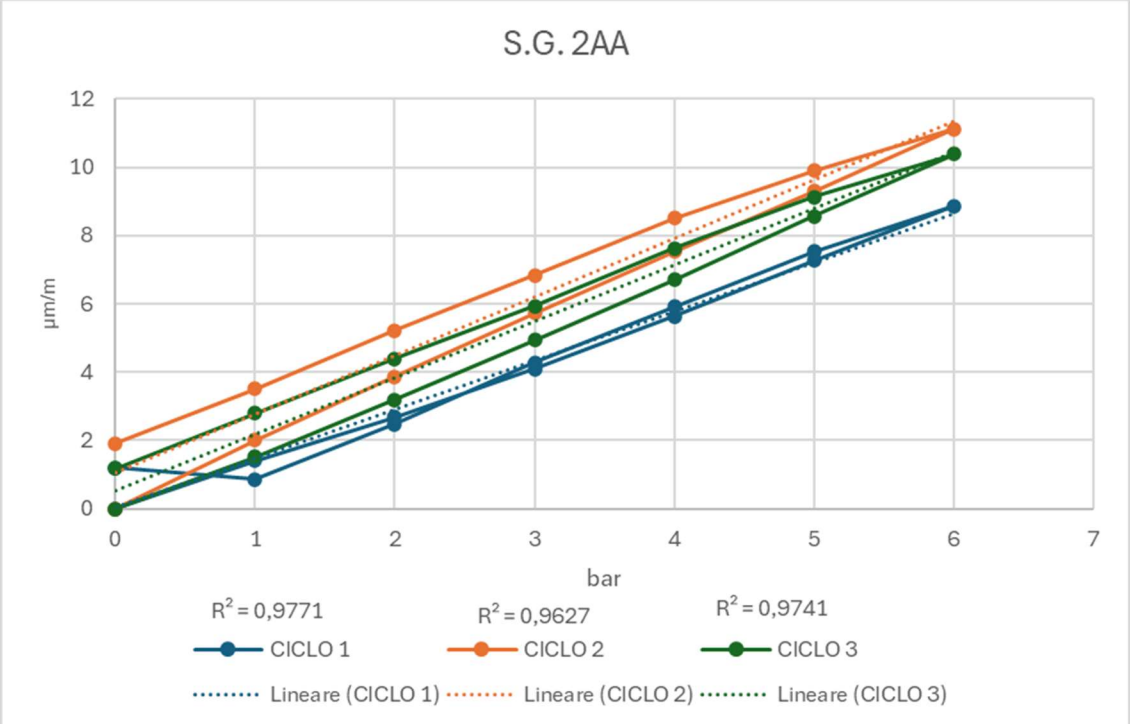

Figure 35: 2AA strain gauge results - axial

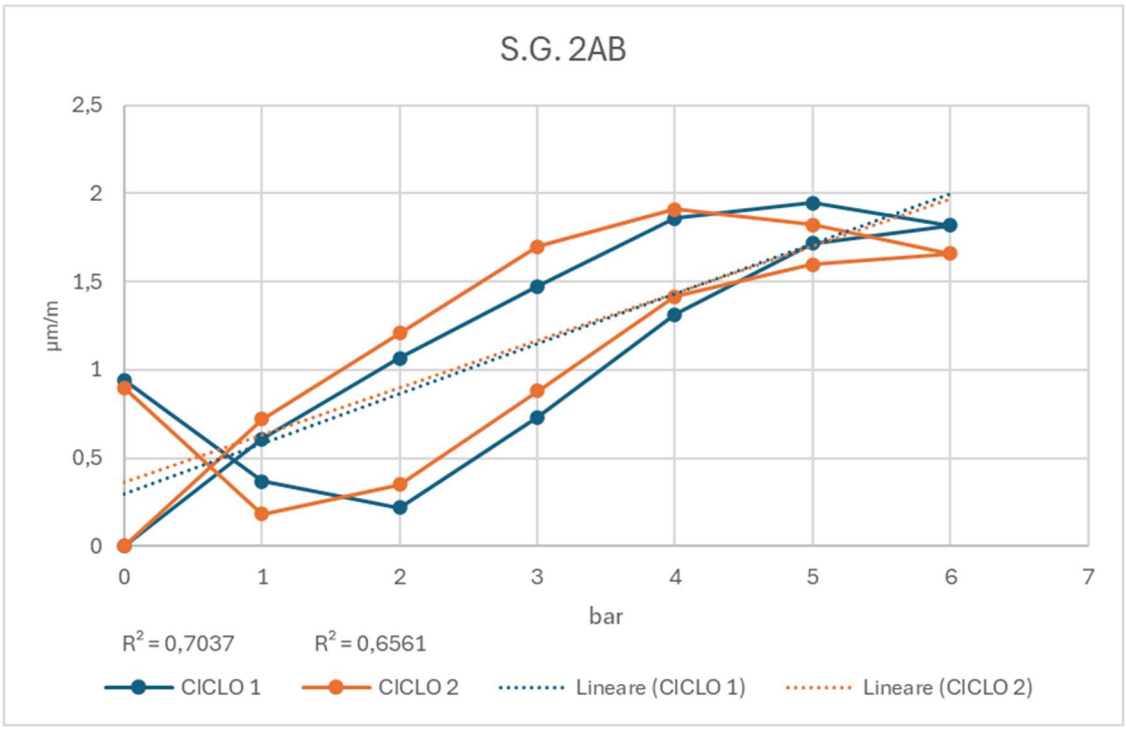

Figure 36: 2AB strain gauge results - axial.

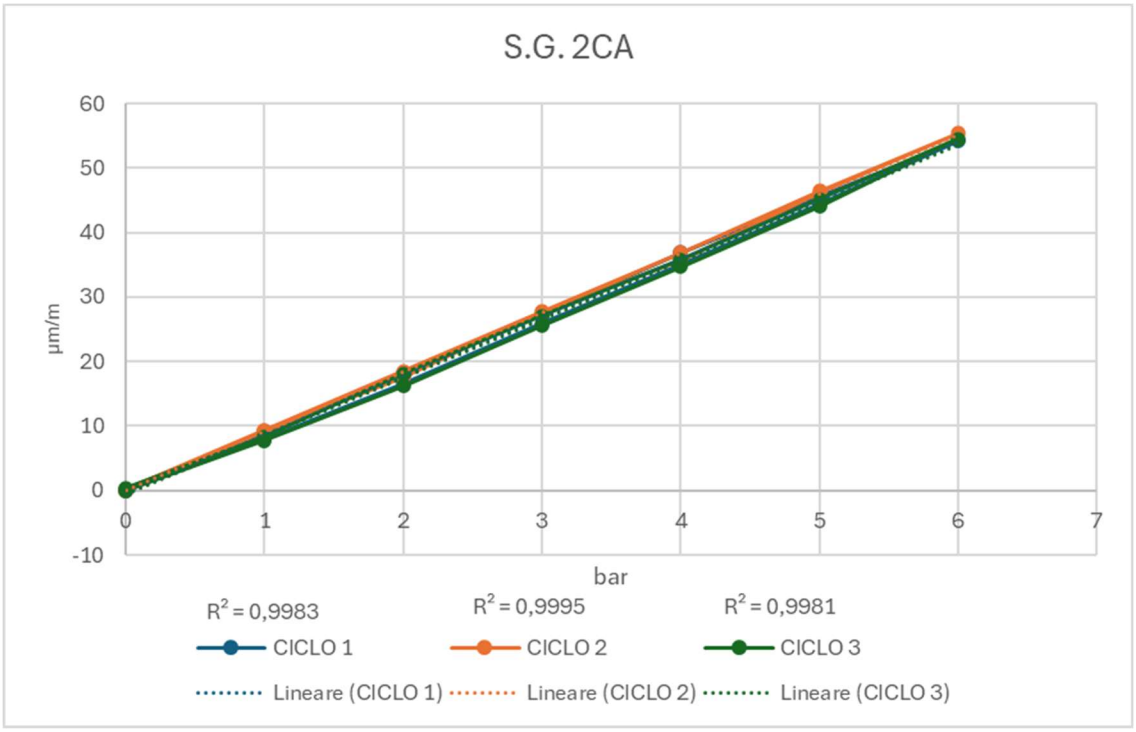

Figure 37: 2CA strain gauge results - circumferential.

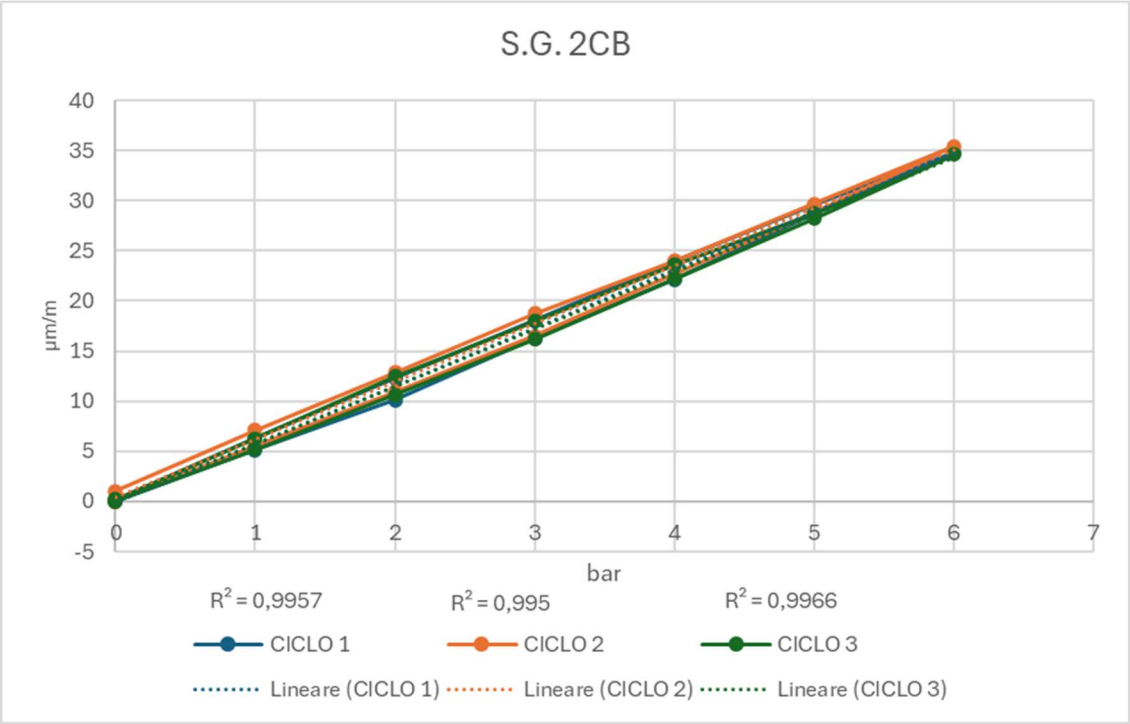

Figure 38: 2CB strain gauge results - circumferential.

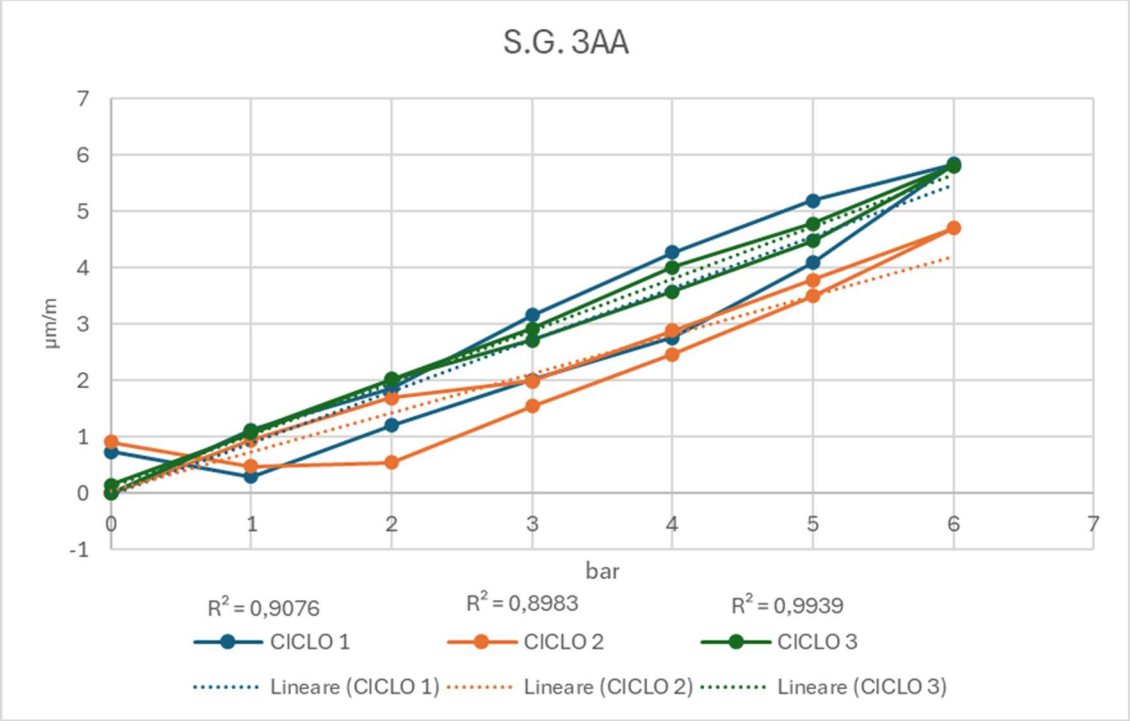

Figure 39: 3AA strain gauge results - axial.

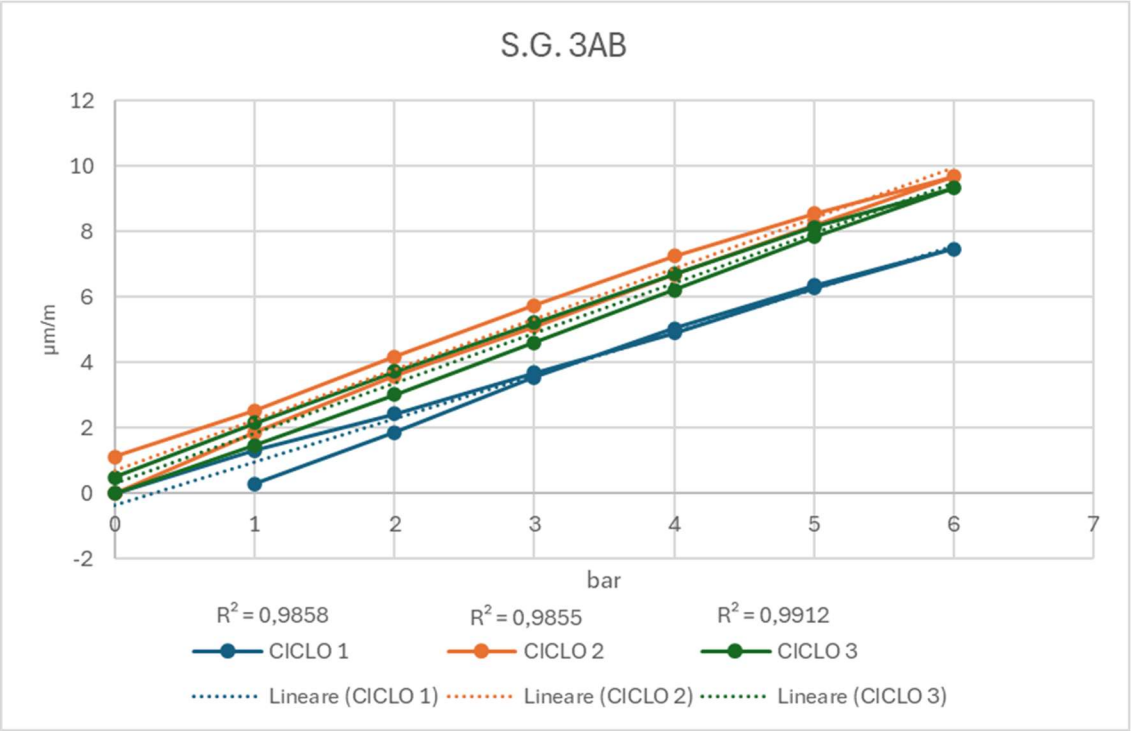

Figure 40: 2AB strain gauge results - axial.

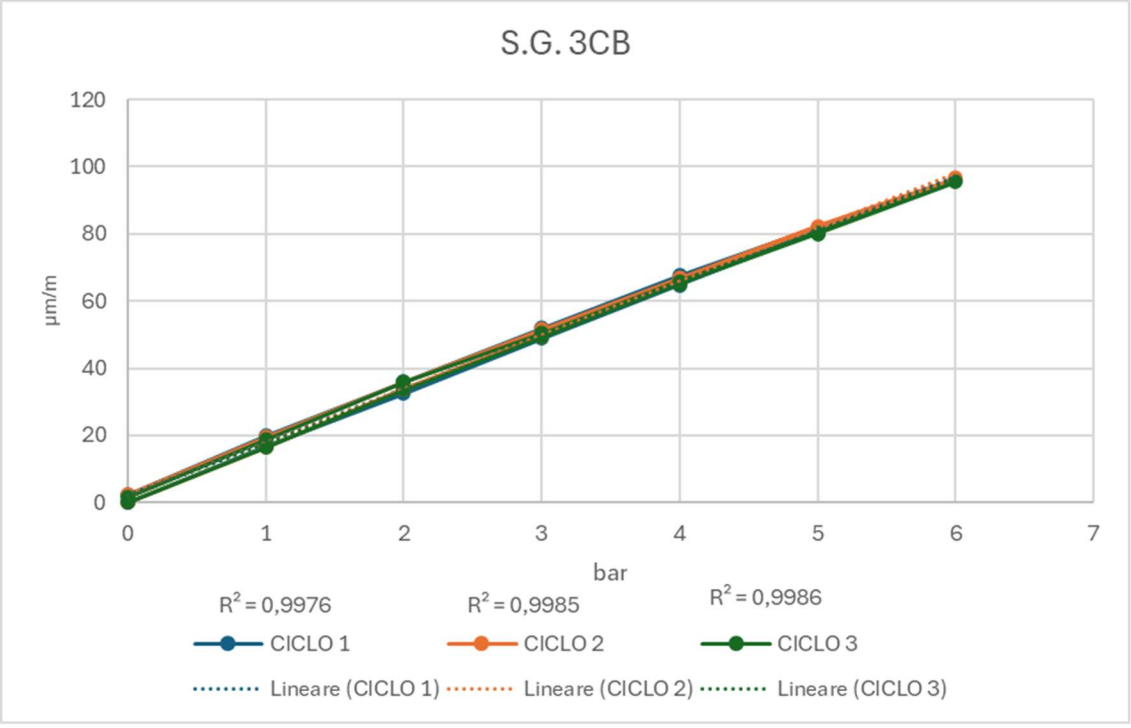

Figure 41: 3CB strain gauge results - circumferential.

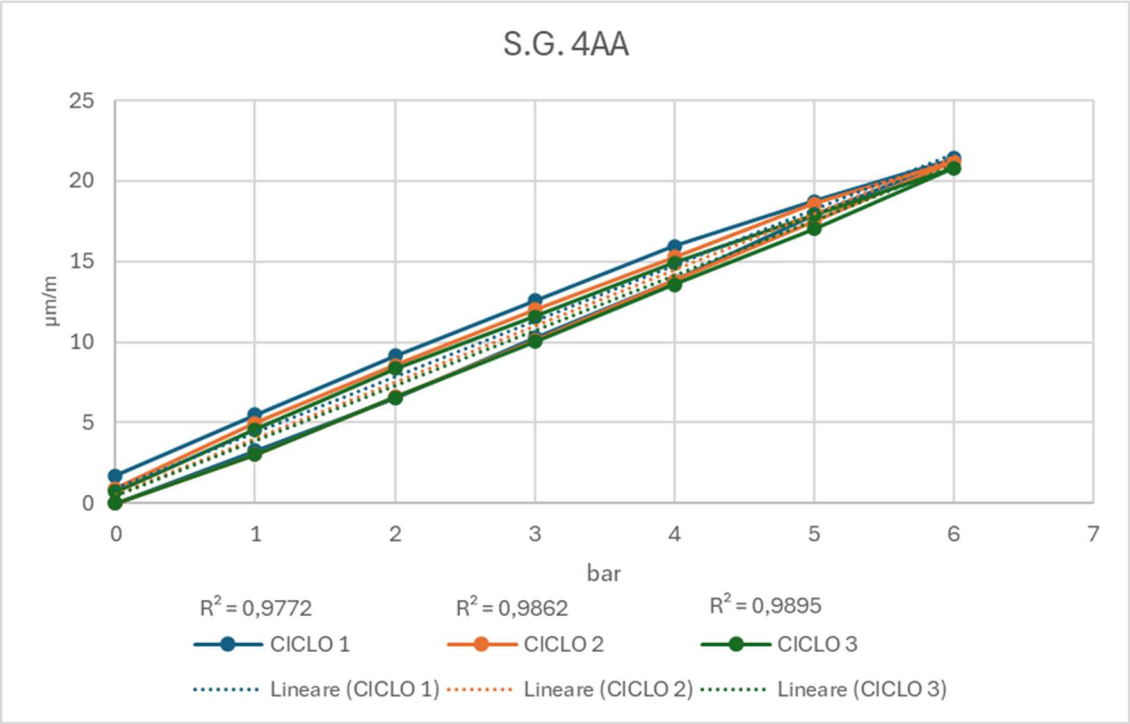

Figure 42: 4AA nozzle strain gauge results - axial.

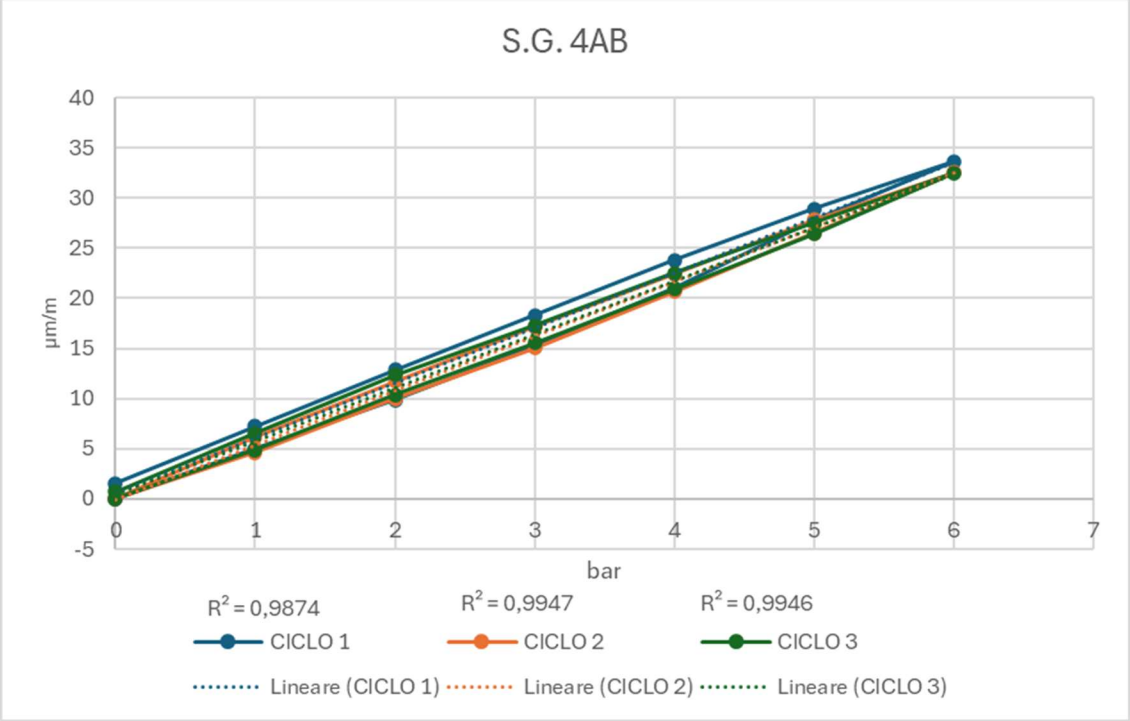

Figure 43: 4AB nozzle strain gauge results - axial.

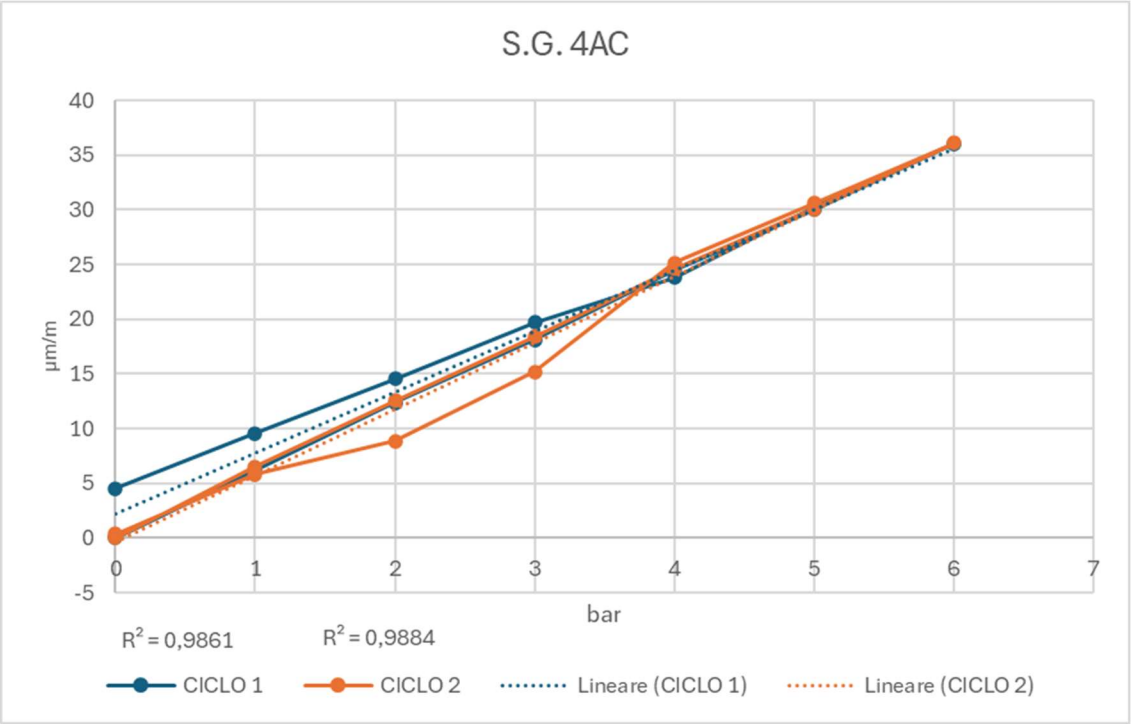

Figure 44: 4AC nozzle strain gauge results - axial.

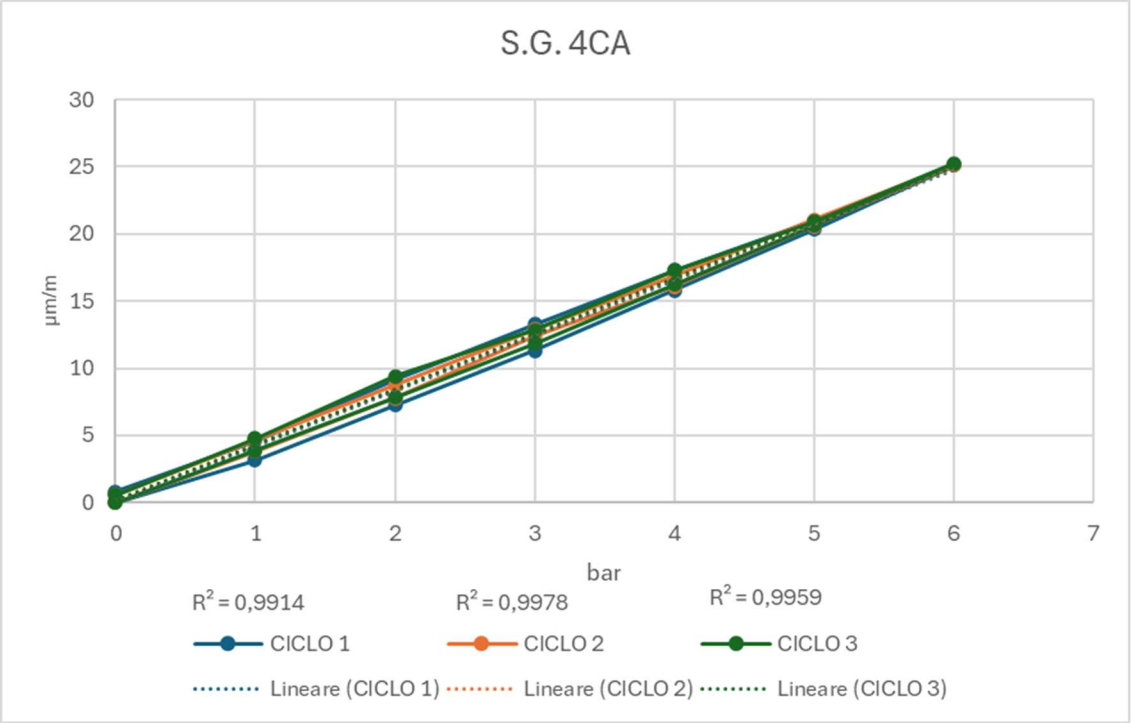

Figure 45: 4CA nozzle strain gauge results - circumferential.

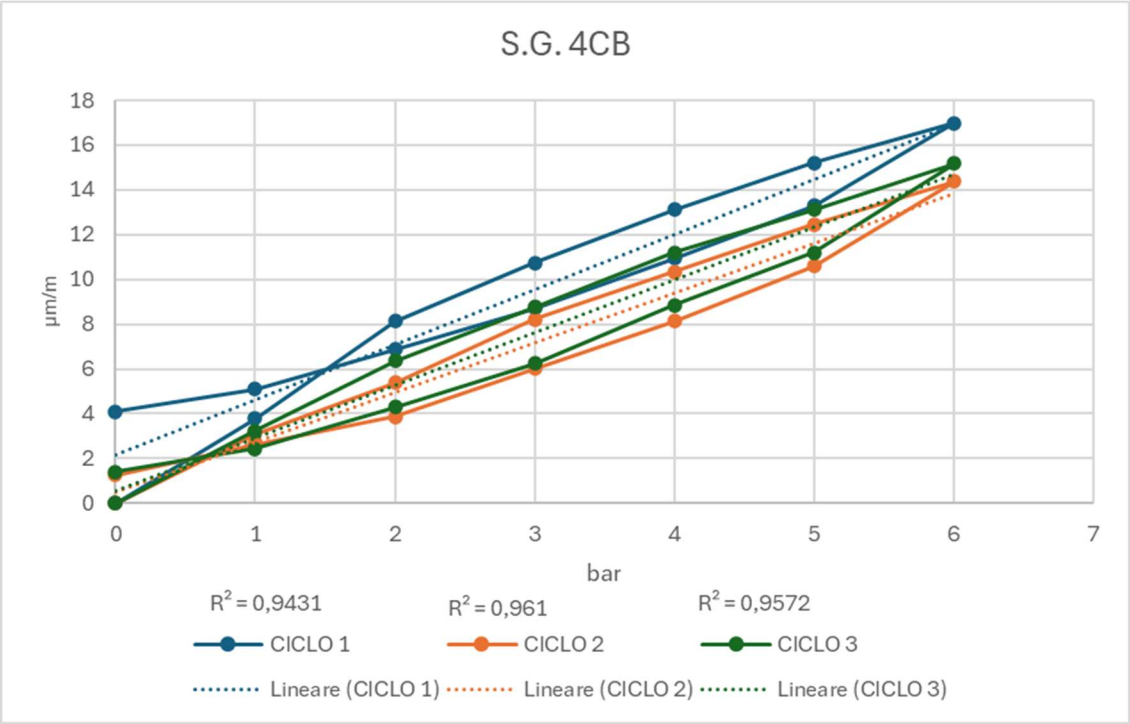

Figure 46: 4CB nozzle strain gauge results - circumferential.

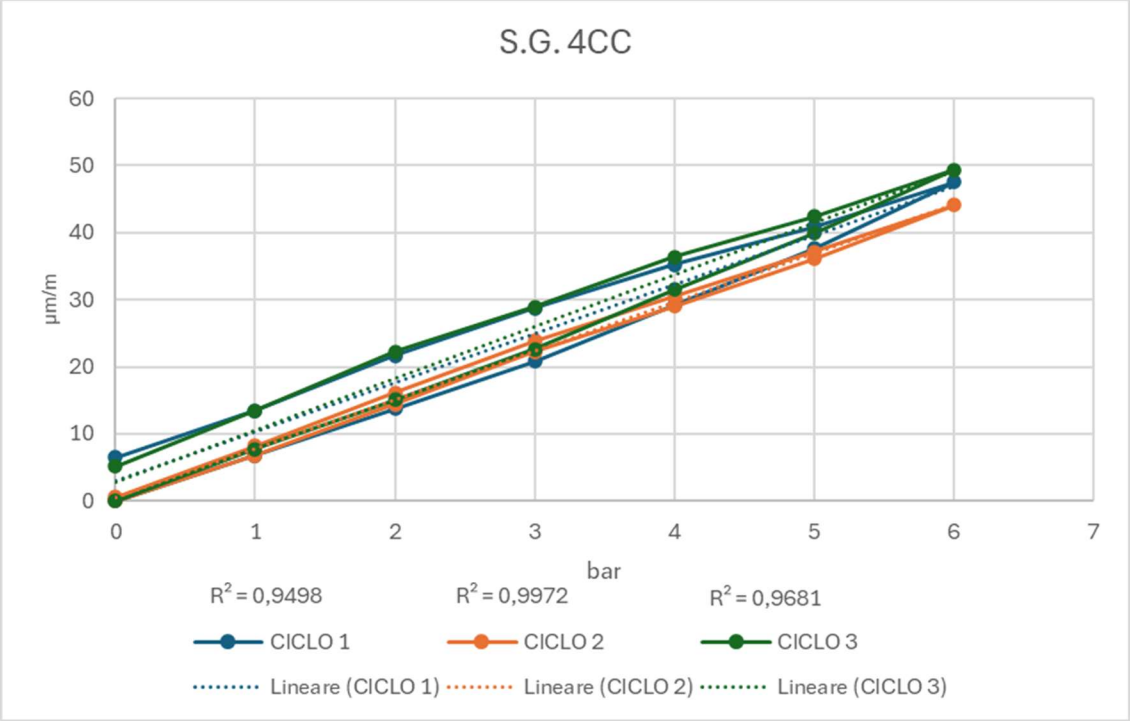

Figure 47: 4CC nozzle strain gauge results - circumferential.

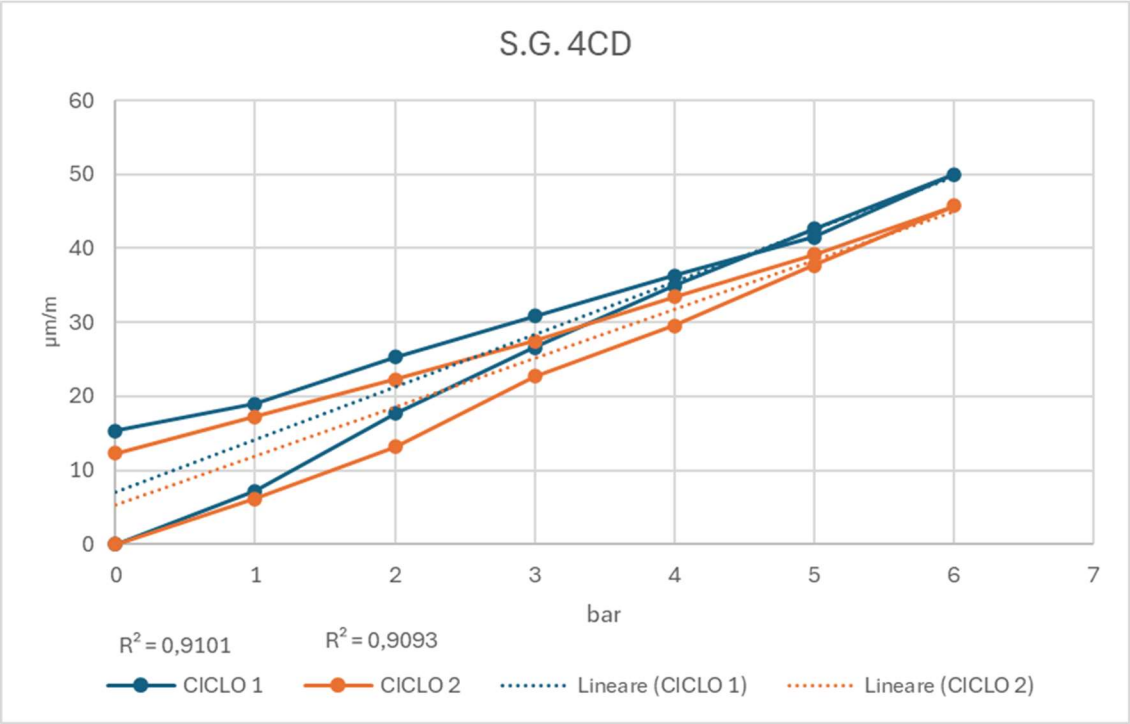

Figure 48: 4CD nozzle strain gauge results - circumferential.

As previously mentioned, the results from some strain gauges were not reported as they were deemed extremely unreliable. This could also apply to strain gauge 2AB (Fig. 36), whose results show significant hysteresis and are much smaller compared to the others, however, they are not discarded because, unlike the others, they do not show significant oscillations.. Regarding the other graphs, the deformations are within the expected order of magnitude in mn, and furthermore, as deduced from the FEA, unlike theoretical formulas, the deformations vary from point to point.

From the graphs of the experimentally measured deformations, it is possible to observe the difference from the FEA results, which are of the same order of magnitude but significantly smaller. As mentioned in the previous chapter, the FEA results need to be calibrated and validated against experimental results. Therefore, the differences between the FEA model and the experimental model are compared, as was done previously.

Regarding the model's geometry, FEA often simplifies it compared to reality. This is because the CAD models used are idealized: surfaces are represented as perfectly smooth, with sharp edges and no internal defects or variations in thickness. In reality, however, physical components may have manufacturing tolerances, imperfections, surface roughness, or internal defects that affect their behavior under load.

Additionally, the approximations made in modeling the connections between components, such as welds, may not accurately represent the complexity of real behavior. These factors can contribute to discrepancies between the results.

The material properties used in FEA often come from standardized laboratory data or literature. These data may not reflect the exact conditions of the material used in the experiment. For instance, a material might exhibit anisotropy (different properties depending on the direction) or variations in properties due to heat treatment, manufacturing processes, or exposure to different environmental conditions.

Moreover, FEA generally assumes that materials are homogeneous and isotropic (as do theoretical formulas), but in reality, materials can have inclusions, density variations, or other heterogeneities that affect their behavior under load.

As previously mentioned, the mesh is a crucial component of FEA and influences the quality of the results. A well-defined and adequately refined mesh can capture fine details and local behaviors such as stress concentration, thus closely matching the experimental results.

In the case of ANSYS Student, for example, the number of nodes and elements is limited, as previously mentioned. This limits the ability to create a sufficiently fine mesh to capture the smallest details and critical regions of the model. This limitation can lead to a reduction in the accuracy of the results, especially in areas with strong stress or deformation gradients.

Boundary conditions in FEA are often idealized. For example, a support constraint may be modeled as completely fixed (no movement), whereas in reality, there may be some flexibility or play. These small movements can have a significant impact on experimental results but are not captured in the FEA model.

FEA applies loads in a precise and uniform manner, but in reality, loads may be distributed unevenly or influenced by environmental conditions such as vibrations or temperature variations.

Many materials do not exhibit linear elastic behavior under load. They may exhibit phenomena such as plasticity, creep, and viscoelastic behavior. Although FEA can model these nonlinear behaviors, doing so accurately requires a deep understanding of the material properties and precise loading conditions. Thus, errors in modeling these behaviors can lead to discrepancies from the experimental results.

Contacts between surfaces are difficult to model accurately in FEA, especially if they include friction, adhesion, or phenomena like play between components. These

aspects are often simplified in the FEA model, but they can significantly impact experimental results.

In turn, real experiments may be subject to measurement errors, variations in test conditions, or human error. The instruments used in experiments may also have precision limits that affect the results. For example, a loss of connection to the acquisition board, even for a few seconds, renders the results of that specific measurement cycle unreliable and thus subject to being discarded.
Discrepancies between FEA and experimental results are inevitable, but understanding these differences is crucial for correctly interpreting FEA results and using them effectively in the analysis process. Therefore, experimental results are considered the most accurate, followed by FEA results, and finally, theoretical results.

Measurements of deformations in the head and liquid level in the vessel

The installation of strain gauges on the lower spherical cap can be used to read the deformations but also to understand how the container would react if it were not pressurized but only water was present inside. In particular, we try to find a sort of correspondence between the height of the water inside and the deformation undergone by the cap.

First, we proceed with the exposition of the physical phenomena involved.

This force will produce the tension responsible for the deformation. This tension will be proportional to P but will also depend on the mechanical properties of the shell material and the geometry.

The tangential (or "membrane") stress in a spherical shell, as explained above, can be expressed using the formula as:

$$\sigma = \frac{PR}{2t} \quad (22)$$

Where:

- P is the pressure (MPa),
- R is the radius of the cap (m),
- t is the thickness of the cap (m).

The deformation associated with this tension is given by Hooke's law for elastic deformation used whether the vessel was pressurized or simply filled:

$$\varepsilon = \frac{\sigma}{E} \quad (23)$$

where E is Young's modulus expressed in MPa .

In an unpressurized tank, the hydrostatic pressure exerted by the water on the lower cap depends on the height of the water column. The hydrostatic pressure at depth is given by the following equation:

$$P = \rho g H \quad (24)$$

Where:

- $\rho$is the density of water (about 1000 kg/m ^{3}),
- g is the gravitational acceleration (about 9.81 m/s ^{2}),

- H is the height of the water column above the point considered.

This pressure is distributed evenly across the entire surface of the shell, increasing proportionally with the height of the water.
The total force F exerted on the lower cap is obtained by integrating the pressure over its entire surface. If we consider a hemispherical cap of radius R, the force acting on an infinitesimal element of the area of the cap depends on the local pressure, which varies with depth.
So, considering the formula (22), (23), (24) expressed above, we get:

$$\varepsilon = \frac{\rho g H R}{2tE} \quad (25)$$

A spherical cap, compared to a flat one, resists pressure better due to its shape. The membrane tension, in fact, distributes the pressure over a larger surface, reducing the overall deformation and the deformation is lower than a flat plate. *(Sesana, 2023)*
From the theoretical formula (13) the deformations for the different pressure levels are calculated (Tab. 4).

P (bar)	ε
0	0
1	1,3E-05
2	2,6E-05
3	3,89E-05
4	5,19E-05
5	6,49E-05
6	7,79E-05

Table 4: Deformations on the spherical cap.

Theoretical formulas would suggest that the deformations should be equal on all points of the lower shell and independent of the direction, whether axial or circumferential; however, in a real shell this does not happen, for various reasons related to the physical reality of the component.
First of all, it should be specified that, as with any material subjected to processing, these components are never perfectly made and may present imperfections such as variations in thickness, non-uniformity of the material or irregularities in the curvature.
The presence of constraints and boundary conditions (which in this case are represented by the support feet) modifies the deformation behavior in the close proximity. Similarly, openings such as the nozzle present modify the distribution of

deformations generating stress concentrations. This effect must be considered in superposition to the residual deformations introduced by the welding process, so it would be expected that these areas present a different response to the stresses compared to the other points of the cap.

The results obtained from the pressurization cycles are represented as before by plotting the stress-strain curves for both the loading and unloading phases in order to visualize the hysteresis cycles (Fig. 49 to 52). Furthermore, for each cycle the R2 index is reported, which indicates the deviation of the strain from the linear trend: a value closer to 1 indicates a smaller deviation and therefore a greater amplitude of the hysteresis cycle.

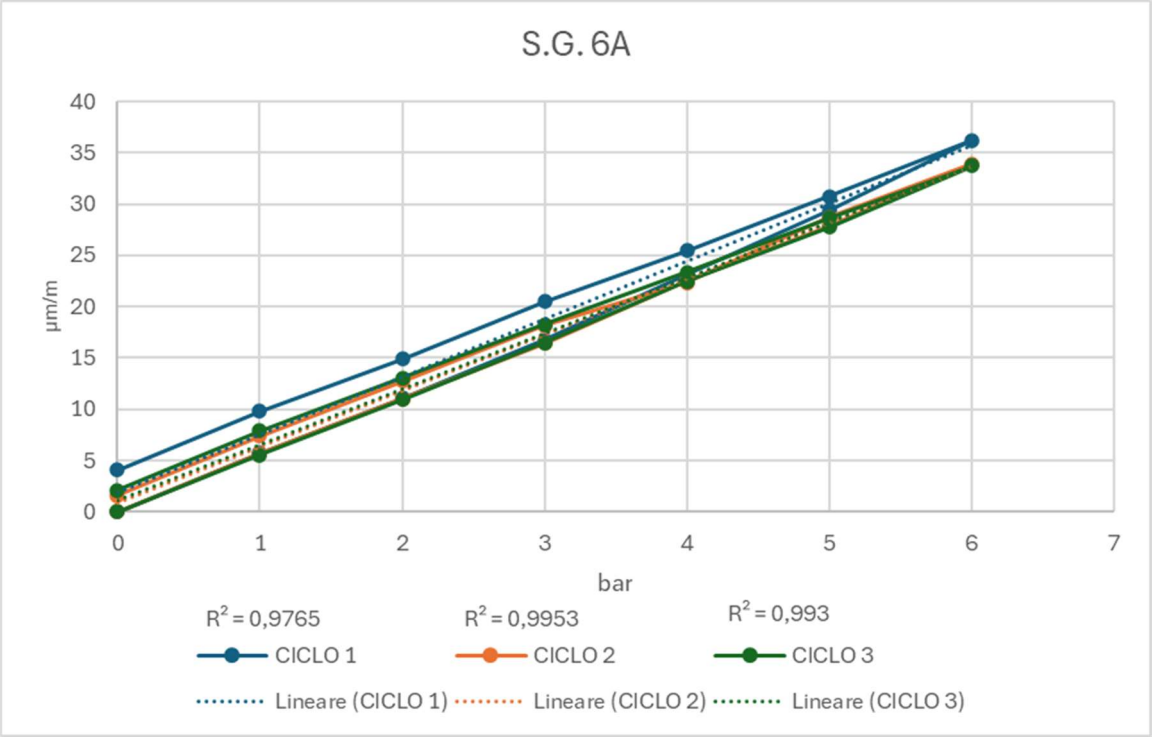

Figure 49: 6A dome strain gauge results .

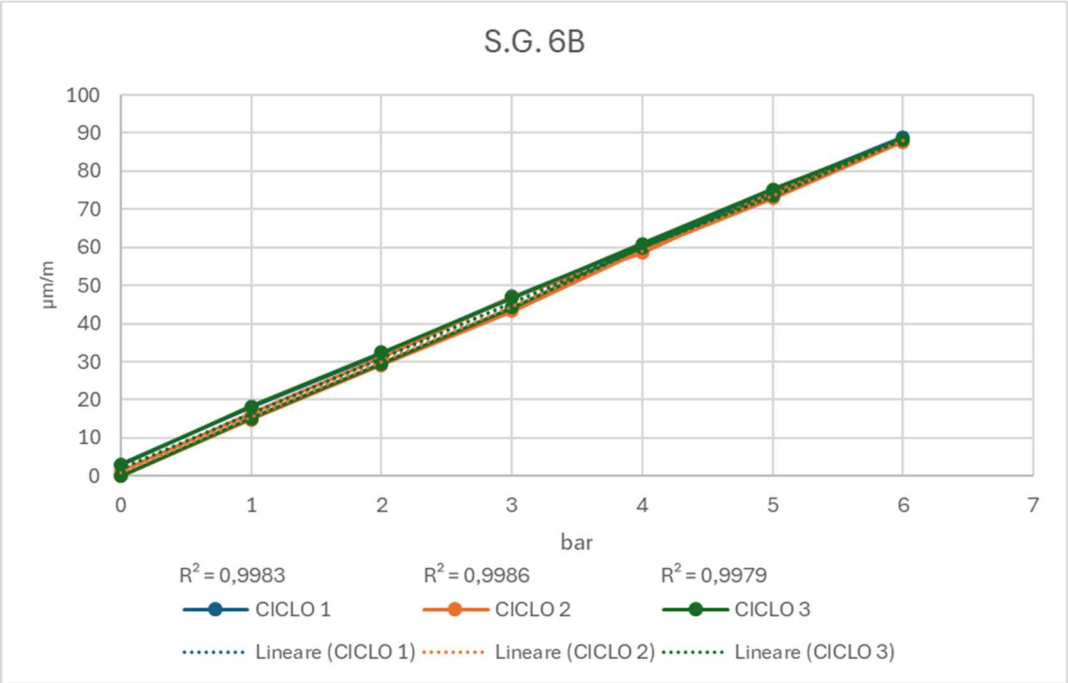

Figure 50: 6B dome strain gauge results .

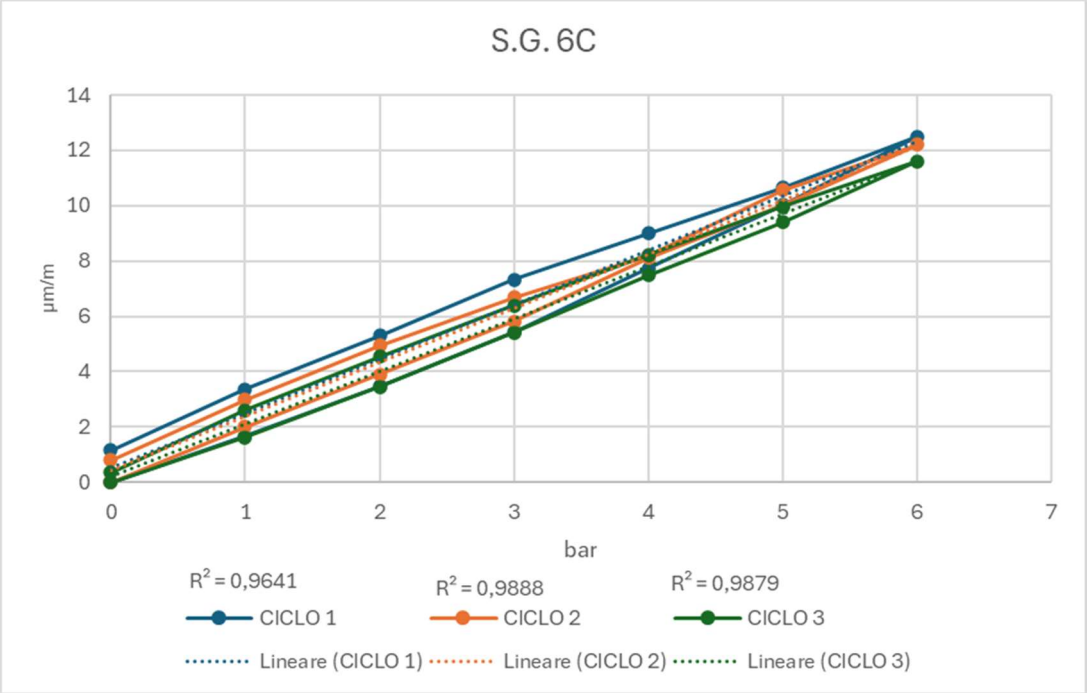

Figure 51: 6C dome strain gauge results .

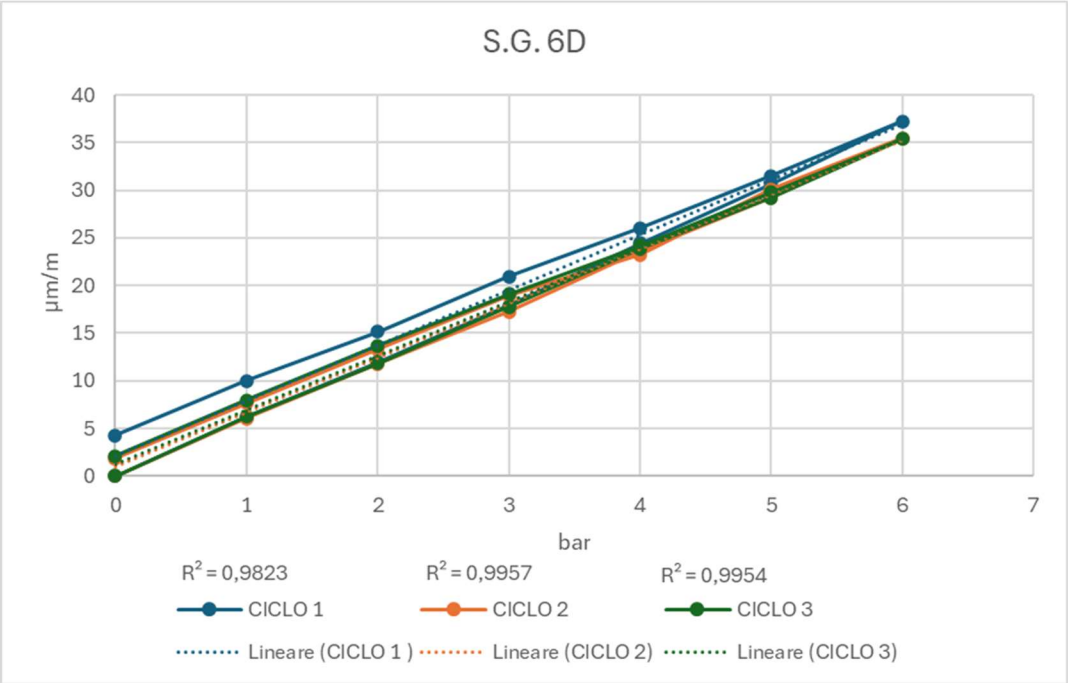

Figure 52: 6D dome strain gauge results.

The strain gauge that shows results that are closest to the theoretical ones is the '6B', both in terms of values and with regards to the R^2 index.

To measure the water level, a small transparent tube is added to the vessel and connected to a tap at the bottom which is kept open (Fig. 30) so that the water level inside the tube is always the same as inside the container.

The tube is then fixed on the side of the vessel and notches are represented to recognize the height, in particular starting from the upper circumferential weld every 15 cm a reference point is placed. Therefore for the height of 60 cm of the shell 5 reading points are placed up to the lower circumferential weld. From here on we proceed with the reading of the last step.

For ease of execution, these readings are taken during the emptying phase, keeping the strain gauges constantly connected to the acquisition card.

The results obtained from the calculations based on the theoretical formula obtained (25) are reported in (Tab. 5)

1000	rho (kg/m3)		H (m)	ε
9,81	g (m/s2)		0,784	9,98E-07
0,1495	R (m)		0,692	8,81E-07
3,00E-03	t (m)		0,542	6,90E-07
0,092	h head (m)		0,392	4,99E-07
0,15	step (m)		0,242	3,08E-07
0,6	h shell (m)		0,092	1,17E-07
192000	E (MPa)		0	0,00E+00

Table 5: Results from the theoretical formula with only hydrostatic pressure.

These are compared with the strains read using strain gauges (Tab. 6)

H (m)	ε 6A	ε 6B
0,784	3,507	1,423
0,692	2,375	0,783
0,542	1,54	0,501
0,392	1,236	0,301
0,242	0,299	0,282
0,092	0,141	0,049
0	0	0

Table 6: Results from the strain gauges with only hydrostatic pressure.

It is possible to note how, also in this case, the strain gauge '6B' presents smaller deformations than the '6A'. This may be due, as previously mentioned, to the proximity of the former to the nozzle and therefore to a possible influence of the welding on the mechanical resistance of the material.

The experimental and theoretical results are compared on a deformation-water height graph (Fig.53) and it is visible that the behaviour which comes closest to the theoretical one is again that of the strain gauge '6B', which can therefore be considered the most accurate of the 4 present on the cap.

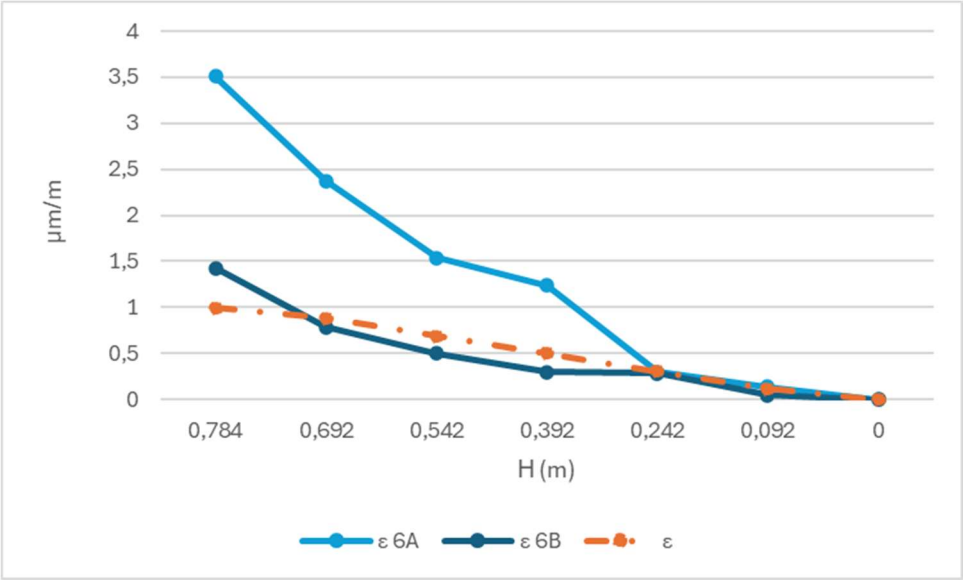

Figure 53: Experimental results compared with theoretical ones.

Appendix A

Figure 54: Photo from laboratory 1

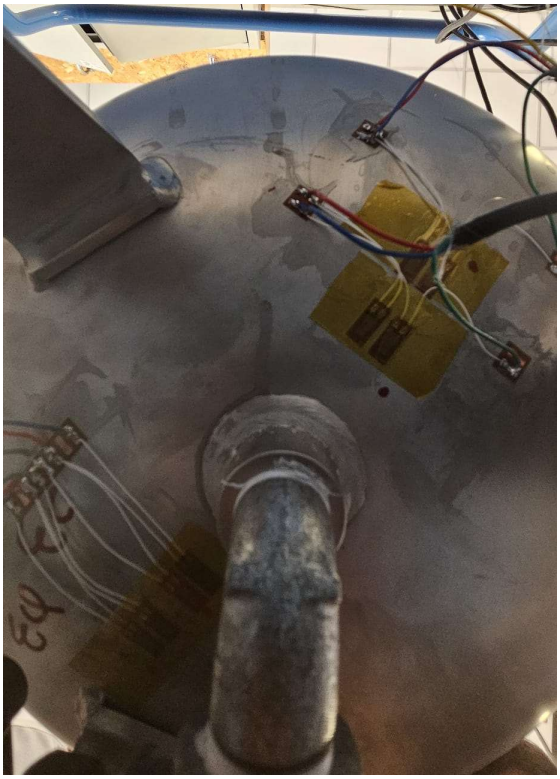

Figure 55: Photo from laboratory 2

Figure 56: Photo from laboratory 3

Figure 57: Photo from laboratory 4

Figure 58: Photo from laboratory 5

Figure 59: Photo from laboratory 6

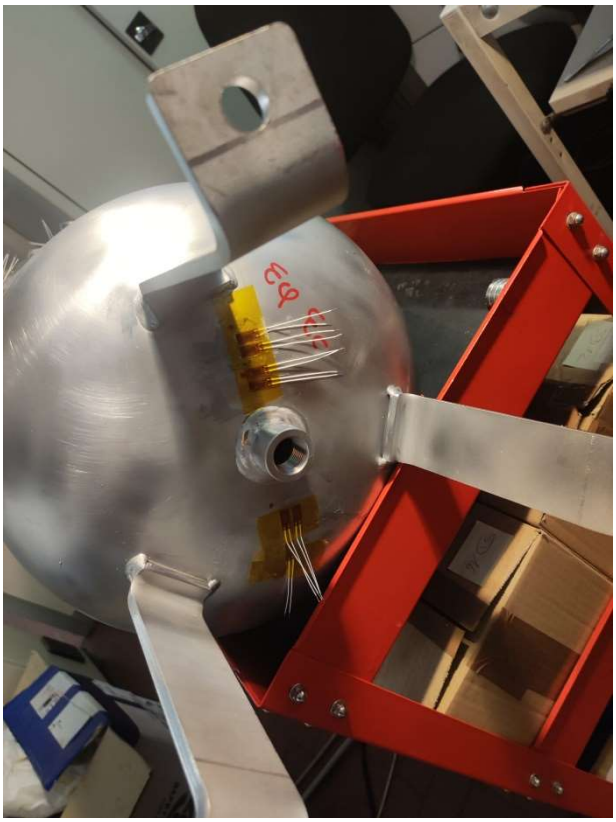

Figure 60: Photo from laboratory 7

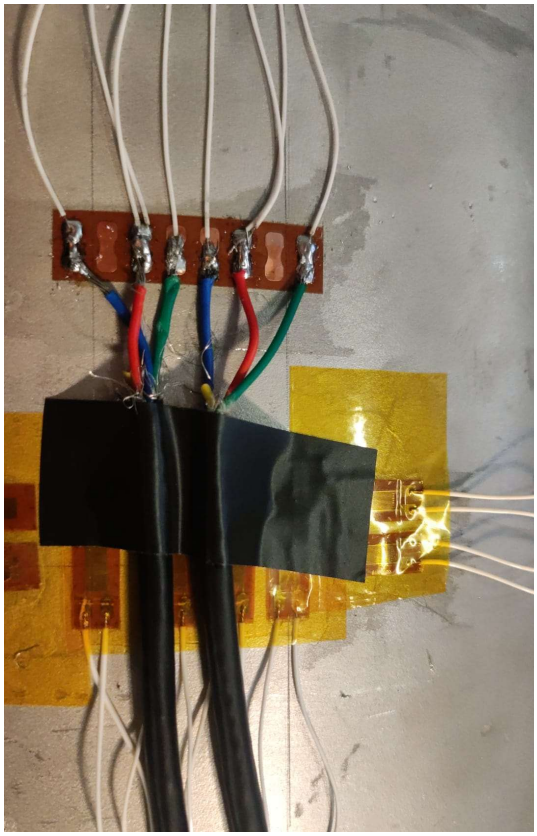

Figure 61: Photo from laboratory 8

Bibliography

Baglioni Group. (n.d.). ***Since 1968, Italian design for worldwide pressure solutions*.** https://www.baglionispa.com/about-us/history

Baglioni Group. (2023). **Serbatoi a Pressione - *CATALOGO*.** https://baglionispa.com/serbatoi/

Sesana, R. (2023). **Thermal machines and structural mechanics** [PowerPoint slides]. Politecnico di Torino.

HBM. (n.d.). **Amplificatore per estensimetri – QuantumX MX1615B / MX1616B.** https://www.hbm.com/it/3053/quantumx-mx1615b-bridge-amplifier-for-strain-gauges/?product_type_no=Strain%20Gauge%20Amplifier%20QuantumX%20MX1615B/MX1616B

HBM. (n.d.) **LY: Estensimetri Lineari con 1 Griglia di Misura.** https://www.hbm.com/it/4561/ly-estensimetri-lineari-con-1-griglia-di-misura/?product_type_no=LY%20Estensimetri%20Lineari%20con%201%20Griglia%20di%20Misura

Ortombrina, L. (2013). **Sistema di misurazione per tensioni superciali di una trave in acciaio tramite strain gauge** (Tesi di Laurea). Università degli Studi di Padova.

Gobbi, A. (2012). **Sensori di forza e coppia per macchine automatiche**. (Tesi di Laurea). Università degli Studi di Padova. https://thesis.unipd.it/retrieve/41fb0fe8-1430-4a05-95ad-8f6dae3361e1/Tesi_di_Laurea_Gobbi_Alberto.pdf

Cazzato, M. (2018). **Studio di fattibilità di un banco prova per organi di trasmissione**. (Tesi di Laurea Magistrale). Politecnico di Torino. https://webthesis.biblio.polito.it/8111/

Bonfanti, A. (2020). **Misure estensimetriche su componenti meccanici**. (Tesi di Laurea Magistrale). Politecnico di Torino. https://webthesis.biblio.polito.it/14157/

Abdolreza, T. Tan Wai, H. (2019) **A critical review and analysis of pressure vessel structures.** *IOP Conf. Ser.: Mater. Sci. Eng.* 469 012009 https://iopscience.iop.org/article/10.1088/1757-899X/469/1/012009